Technische Universität München

Fakultät für Medizin

Studies on cellular autophagy and lipid droplet induction in Mesenchymal Stem Cells from type 2 diabetes patients after low dose X-irradiation

Jing Wang

Vollständiger Abdruck der von der Fakultät für Medizin der Technischen Universität München zur Erlangung des akademischen Grades

Doktors der Medizin (Dr. med.)

genehmigten Dissertation.

Vorsitzender: Prof. Dr. Jürgen Schlegel

Prüfer der Dissertation:

1. Prof. Dr. Hans-Günther Machens

2. Prof. Dr. Michael John Atkinson

Die Dissertation wurde am 16.07.2020 bei der Technischen Universität München eingereicht und durch die Fakultät für Medizin am 03.11.2020 angenommen.

Table of Content

Abstract

Type 2 Diabetes mellitus (T2D) is one of the most prevalent diseases in the modern civilization and responsible for about 200.000 cases of death in Germany. The annual costs for the treatment of this chronic disease is about 35 billion Euro in Germany. Most of the T2D complications responsible for the costs and for the shortened life expectancy are caused by comorbidities affecting the broad range of tissues and organs in patients with T2D.

One of the most common secondary complications caused by type 2 diabetes mellitus (T2D) leading to disabilities and earlier death are cutaneous wound healing complications. In this study I tried to better understand the relationship between mesenchymal stem cells, their role in normal wound healing and the molecular defect that affects their function in T2D patients. Mesenchymal stem cells (MSCs) have been shown to provide therapeutic value for tissue regeneration and wound healing. However, under chronic pathological conditions, T2D-MSCs have been functionally altered due to long-term exposure to systemic and local high blood glucose stem cell microenvironment.

Autophagy plays an essential role in the treatment of disease with MSC from different sources. Autophagy exists in normal cells components such as abnormal intracellular proteins, damaged organelles, and lipid droplets degraded by special pathways of autophagy lysosomes. Lipid droplets are identified as organelles that store neutral lipids in eukaryotic cells. A growing number of studies have indicated that in addition to serving as the main storage sites for intracellular triglycerides and cholesterol, lipid droplets can also interact with other organelles and participate in many biological cellular processes of cells. Autophagy is closely related to diseases caused by metabolic disorders such as type 2 diabetes and obesity. Many studies have found that mammalian target of rapamycin (mTOR) pathway is impaired and autophagy is inhibited in type 2 diabetes. Autophagy plays a certain role in lipid drop homeostasis. Inhibition of autophagy leads to the accumulation of triglycerides and lipid droplets,

while induction of autophagy leads to a decrease in number of lipid droplets. By activating autophagy, bone marrow mesenchymal stem cells can alleviate the damaged cells induced by chronic hyperglucose-induced injury and reduce the severity of ischemia (J. Li et al., 2015).

This study aims to find out differences between T2D-MSCs and healthy-MSCs when exposed to 3 Gy radiation, and to generate MSCs with therapeutic potential from T2D patients derived stem cells, thereby reducing cell heterogeneity and age-related impairment of stem cell potency.

After the treatment with 3 Gy radiation, degrees of autophagy ability, lipid-droplets formation, senescence and DNA repair foci formation were quantified by using cytochemistry and immunofluorescence. T2D BMSCs have more cells with lipid-droplets and less senescent cells than healthy BMSCs after being exposed to 3 Gy radiation. The profiles of γH2AX foci formation after 1.5 hours haven’t shown any difference between T2D and healthy donors. The acquired LC3B signals of T2D donors show autophagy resistance.

1 Introduction

1.1 Type 2 diabetes as a disease of the affluent society

The prevalence of diabetes mellitus has rapidly increased globally with the changes in human living habits and diet structure, which have brought many adverse effects on human life and reduced people's quality of life (Orozco-Beltran et al., 2016; Shaw et al., 2010).

Diabetes mellitus is divided into two types, primary and secondary. 95% of people with diabetes are secondary, type 2 diabetes. According to the forecast of relevant departments, the incidence of type 2 diabetes will climb to 459 million people in 2030. In the aging and industrialized population, overweight and lack of exercise due to urban modernization have become the main causes of type 2 diabetes (Shaw et al., 2010). Hypertension, dyslipidemia, and other factors also increase the risk of illness.

1.2 Costs and challenges inflicted by T2D secondary health complications

Type 2 diabetes has become the third most serious disease that threatens human health after tumors and cardiovascular diseases. This disease obviously affects the patient's quality of life, increases medical expenses, and in severe cases require amputation or even threatens the patient's life. Causing a serious burden on the patient's family and society.

Diabetes mellitus as a metabolic disease that leads to an abnormally high concentration of glucose in the patients' peripheral blood. Type 2 Diabetes (T2D) is primarily a disease of the energy metabolism of higher organisms, characterized by a progressing inability to regulate the blood serum level of glucose and make it available to the cells with a high ATP demand (such as muscle, brain, liver). The underlying reason is the impaired sensitivity of the tissue to respond to insulin in the blood (insulin resistance)(Rao et al., 2019). If unrecognized or untreated, this will lead to a chronic hyperglycemia throughout the organisms, and will eventually result and in a broad spectrum of secondary morbidities. Widespread and chronic systemic inflammation will be observed, and a generalized vasculopathy is obvious on the histo-pathological level in various organs. These vasculopathies involve mainly the

arterioles and sinusoids, which are damaged and respond with inflammation and degeneration. Functional impairments of the microvasculature are considered to be the initial step leading to renal, ocular and cardiac side effects of T2D. Here, degeneration of the micro vessels affects highly sensitive tissues such as the glomeruli of the kidney, the retina of the eyes and the myocardia, resulting in diabetic nephropathy, diabetic retinopathy and T2D associated cardio-vascular diseases (CVD)(Gong et al., 2016; Huang et al., 2006; Y. Li et al., 2018; Yang et al., 2019).

These secondary complications of T2D are the main reason for impaired quality of life, for shortened life expectancy and for the vast majority of diabetes related costs to the health care system.

1.3 Wound healing complications and diabetic foot ulcerations

Diabetic foot ulcers (DFU) are a severe complication of type 2 diabetes. About 15% of diabetic patients will develops DFU, usually at an advance stage of the disease. DFU affects life quality of patients, aggravates the economic burden of patients, and is also one of the main causes of amputation and death of diabetic patients. DFU development is influenced by many risk factors, including age, course of the disease, gender, infection, neuropathy, peripheral vascular disease, smoking, poor blood sugar control, high blood fat rise, glycosylated hemoglobin (HbA1c) level.

There are three factors that ultimately lead to ulceration: peripheral neuropathy, peripheral arterial disease, and repetitive trauma in the same area. Metabolic and neurovascular factors often lead to diabetic neuropathy(Kumar et al., 1994; Tesfaye et al., 1996). The resulting distal nerve damage and low blood flow in the extremities are important causes of further pain or loss of sensation in the toes, feet, legs and arms. Pain or loss of sensation causes small skin lesions to be ignored by the patient, thus becoming a gateway for pathogenic microorganisms that enter the body and leading to a chronic wound inflammation with reduced capacity for healing. Peripheral sensory neuropathy, autonomic sensory neuropathy, and motor neuropathy are identified as the characteristics of neuropathy diabetic foot’s pain insensitivity, foot deformity and skin changes. Healing of skin lesions at areas that are already affected by neuropathic

conditions (reduced haptic sensitivity or nociception) is severely impaired. It can lead to chronic skin ulcers and in later stages often require limb amputation. The possibility that peripheral polyneuropathy and cutaneous wound healing complications simply occur coincidentally as a result of the same causation (such as the vasculopathy affecting the micro-capillary) is shown in Figure 1, Figure 2 (Katsilambros N, 2010). In particular microvascular degeneration caused by chronic hyperglycemia in diabetic patients could be the underlying tissue complication that later give rise to both sensory neuropathy and cutaneous symptoms.

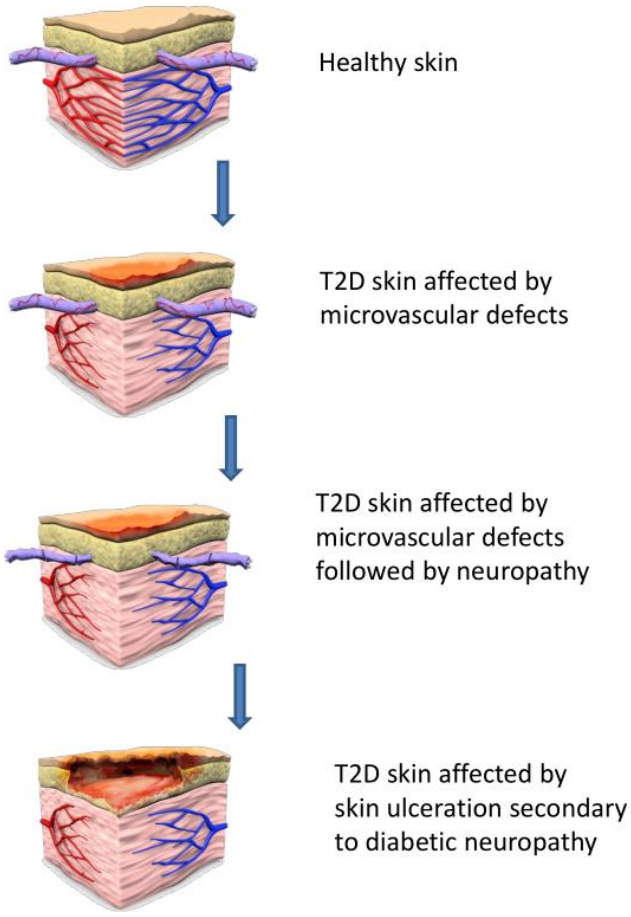

Figure 1: Diabetic skin ulceration secondary to diabetic neuropathy

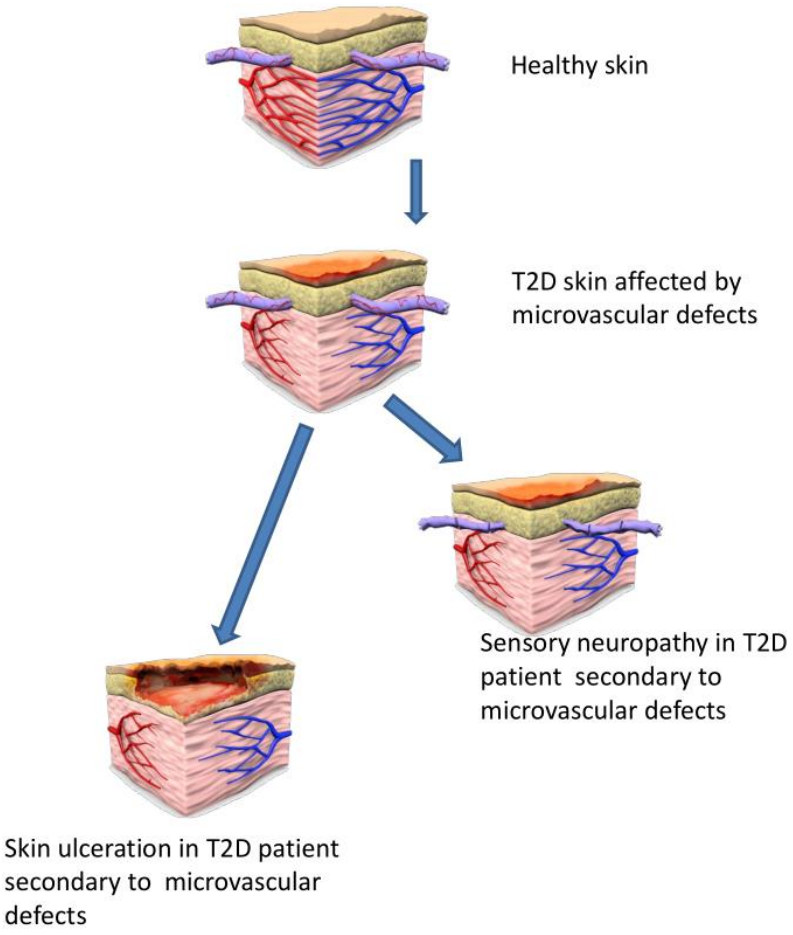

Figure 2: Pathogenesis of diabetic skin ulcerations a mechanism independent of neuropathy

To sum up, DFU is one of the most common complications of diabetes, which seriously affects the quality of life of patients. It is an effective way to reduce the incidence of DFU, to know the related risk factors of DFU, and then to actively take specific preventive measures.

1.4 Physiological processes in healthy wound healing

Skin trauma is one of the most common surgical diseases. Mechanical, thermal, chemical, and other external factors can cause defects and destruction of the epidermis, dermal tissue, and subcutaneous mucosa to form wounds. Wound healing is a highly coordinated process involving multiple tissue components(P. Li et al., 2018). The skin contains a variety of accessory organs, such as sweat glands, sebaceous glands, blood vessels, lymphatic vessels, and nerves. Therefore, when the skin suffers external damage, it will also cause a series of metabolic disorders due to

the damage of its accessory organs, resulting in concurrent chronic skin damage, such as diabetic foot, vein, or artery occlusion(Jiang et al., 2011).

Wound healing is the process of repairing skin wounds by tissues around the wound, which can be divided into three phases: inflammation phase (hemostasis), proliferation phase (fibrous tissue hyperplasia phase), and remodeling phase (scar formation repair phase)(Lindley et al., 2016).

I. Inflammation phase (hemostasis)

After the wound formed, it enters the inflammation phase. First, cells in injured tissue release vasoactive substances to constrict blood vessels and prevent further bleeding. Fibrinogen forms an insoluble fibrin network.

Platelets, lymphocytes, and granulocytes form blood clots to close damaged blood vessels and form a protective film at the wound to prevent further pathogen contamination. Immune cells around the wound secrete various inflammatory factors, such as tumor necrosis factor (TNF), interleukin (IL), and some other cytokines and growth factors. These cytokines and regulatory signals together promote wound healing(Rehman et al., 2004).

II. Proliferation phase (fibrous tissue hyperplasia phase)

In the hyperplastic stage, endothelial cells in the blood vessel break through the basement membrane and migrate to the area around the wound, dividing to form vascular buds. After that, they connect to form a new vascular pathway, and then further form a vascular network and capillary ring to form granulation tissue.

With the participation of multiple growth factors and cytokines, the wound healing transition from the inflammatory stage to the vascularized granulation stage such as fibroblast growth factor (FGF) to promote angiogenesis and fibroblast division(X. Wang et al., 2010); Epidermal growth factor (EGF) can promote angiogenesis, fibroblast migration, and proliferation, improve collagen deposition, and thus promote wound healing to grow a new and complete skin(Gainza et al., 2015).

III. Remodeling phase (scar formation repair phase)

The remodeling phase is the third stage of wound healing. It mainly remodels tissues of the wound, and after a long period of repair, new skin grows. The transformation of granulation tissue generation to wound re-epithelialization marks the beginning of dermal tissue remodeling. In this process, the disordered extracellular matrix (ECM) composed initially of type III collagen, and elastin was replaced by an ordered ECM composed of type I collagen and elastin fibers, thereby reshaping the elasticity and strength of the dermis(Babu et al., 2001). The formation of a new epidermis covering the wound under the action of various factors, marking the completion of the wound healing process.

1.5 Current clinical approaches to manage T2D wound healing complications

In the previous treatments, debridement, dressing change, surgeries, etc. were often used for conventional treatment of diabetic foot ulcers according to the grade of the disease.

Debridement can be divided into physical debridement, biological debridement, and enzymatic debridement according to the principle of debridement. Physical debridement is divided into (ultrasound, scalpel, hydrodynamic debridement system), and biological debridement includes maggots and worm treatment. Maggots have been used for debridement of pressure ulcers and diabetic foot, which has been proven to be a safe and effective debridement method(Hassan et al., 2014; Lodge et al., 2006).

Dressing change is also the most basic method in the treatment of chronic diabetic wounds. The purpose of dressing change is to drain necrotic tissue to prevent wound damage and infection, thereby removing factors that affect wound healing. Reasonable use of topical growth factor drugs in dressing change and supplementary products and antibiotics can also reduce infection rates and shorten the healing cycle.

Traditional surgical treatment methods include flap transplantation, bone transport, and vascular interventional treatment. Flap transplantation is an important surgical

method for covering chronic wounds. Comparing with skin grafting, it makes the scars lighter and less prone to contracture. Some studies have shown that covering the diabetic foot wounds with perforator flaps significantly shortens the length of hospital stay and the rate of amputation(S. W. Kim et al., 2018; Sung et al., 2018). For chronic diabetic wounds caused by ischemia, vascular interventional treatment is one of the fundamental guarantees to solve the problem(Mu et al., 2015).

1.6 Role of mesenchymal stem cells in normal wound healing

In recent years, with the in-depth study of stem cells, more and more research results show that stem cells can promote wound healing. MSCs can directly give rise to fibroblasts (by asymmetric stem cell division)(Kim et al., 2007), promote the aggregation of macrophages, increase the formation of granulation tissue, and support the regeneration of the accessory organs and blood vessels inside the wound skin (Cao et al., 2005). Therefore, MSCs have an important function in the control of the complex processes during wound healing, to avoid scar formation and to reduce a chronic remodeling of large wounds (such as radiation injury, burns, trauma, surgery, etc.) (Figure 3).

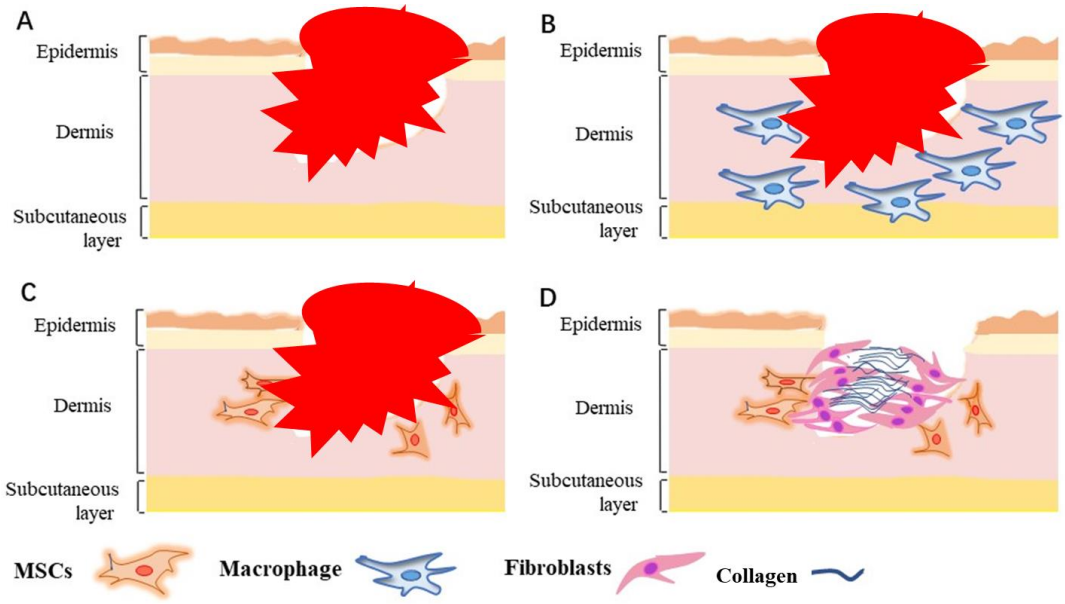

Figure 3: Role of mesenchymal stem cells in normal wound healing

A. Skin injury causing bleeding and wound closure by coagulating blood and fibrin secretion. **B.** Inflammation **C.** Recruitment and homing of MSCs to skin lesion **D.** Closure of lesion by activated fibroblasts and collagen deposition.

MSCs functioning as perivascular MSCs surrounding microcapillaries. They share many characteristics with differentiated pericytes, such as their immunomodulatory and anti-inflammatory activity. In particular, after tissue injury, damage to the microvasculature leads to an activation of the pMSCs, which is considered to be crucial for a well-orchestrated wound healing program. Despite their capability for a long-term proliferation in-vivo and in-vitro, MSCs not necessarily have to generate new precursor cells in order to contribute to tissue repair and regeneration. MSCs are also prominent sources of immuno-modulating and other signaling growth factors.

1.7 Therapeutic applications of mesenchymal stem cells in non-diabetic wound healing

Mesenchymal stem cells have been widely used as an adjuvant for the repair and regeneration of various acute and chronic skin defects, such as acute skin trauma, radiation damage and burns, etc. (Dai et al., 2007; Lataillade et al., 2007; Ren et al., 2019) .

Autologous transplantation of bone marrow derived MSCs (BM-MSC) is effective in patients with non-diabetic wound healing. Its mechanism can be summarized as follows: (1) MSC produced committed precursor or differentiated cells (fibroblasts, vascular smooth muscles cells) and secrete a variety of anti-inflammatory growth factors, such as epidermal growth factor, basic fibroblast growth factor, vascular endothelial growth factor, etc. which promotes wound healing by increasing angiogenesis, tissue regeneration, and recruitment of endogenous stem cells(Chen et al., 2008; Desta et al., 2010; Usui et al., 2008); Supplemental treatment with local MSC applications (autologous derived from patients tissue) has been shown to be highly beneficial for non-chronic, non-diabetic wounds. Patients affected by radiation burns or mechanical wounds show a much advanced and more physiological skin

repair when autologous MSCs are applied in combination with tissue equivalent skin coverings(Larsen et al., 2018; Lataillade et al., 2007).

(2) In addition, MSC transplantation can induce vascular development in ischemic areas and increase capillary density and blood flow. Amann.B et al. used BM-MSCs transplantation to treat patients after severe limb ischemia. However, this method is still in the clinical trial stage, and more clinical trials are needed before it can be wide applied in clinical routine(Amann et al., 2009). From a mechanistic point of view, the interaction between recovery of damaged microvasculature and MSCs is very likely, considering that the perivascular cells (or pericytes), which reside on the periphery of microvessels, are nothing else than MSCs (specifically abbreviated as pMSCs)(Corselli et al., 2012).

1.8 Cellular defects in MSCs of T2D patients

Under chronic pathological conditions, T2D-MSCs may be functionally altered due to long-term exposure to systemic and local stem cell microenvironment. Impaired function of DM-MSC is caused by increased oxidative stress and enhanced inflammatory response(van de Vyver, 2017). Reduced blood circulation (as a consequence of the diabetic vasculopathies) in tissue leads a hypoxia, but also to increased ROS stress and a redox imbalance(Pforringer et al., 2018). The current studies consistently found that diabetic patients had decreased expression of catalase in peripheral blood nucleated cells. Low levels of catalase in blood cells in diabetic patients could enhance oxidative stress (Pan H-Z, 2010). Kim, H et al. showed that osteogenic and angiogenic differentiations of DM-MSCs were abnormal. The expression of angiogenic factors in DM-MSCs was lower and DM-MSCs were ineffective in improving hind limb ischemia (H. Kim et al., 2015). There are also mouse models showing that autologous MSCs from diabetic mice are not effective in supporting wound healing(Shin et al., 2012). If (congenic) MSCs (from healthy mice of the same HLA group) are used, they can support wound healing in diabetic mice. This shows that chronic hyperglycemia damages the MSCs, and using “healthy” MSCs can improve wound healing in a T2D patient.

1.9 Cellular pathways regulating autophagy

This so-called macroautophagy always begins with the formation of autophagosomes, which transport over 30 autophagy protein aggregates and other target substances (such as macromolecules or damaged organelles) to the lysosome for degradation. Long-term studies have shown that the mammalian target of rapamycin (mTOR) is considered as the primary pathway that regulates autophagy, and the representative drug rapamycin (TOR inhibitor) acts as autophagy inducer.

Apart from the so-called Macroautophagy as described above(He et al., 2009), 2 others mechanisms also facilitate degradation of cellular waste products, namely Microautophagy(Sahu et al., 2011; Santambrogio et al., 2011) and Chaperone-mediated autophagy (CMA)(Cuervo et al., 2014). Since they are not in the focus of this research project, their characteristics are only mentioned here briefly to understand the distinct molecular mechanisms.

Microautophagy is characterized by minimal autophagy and is defined as lysosomal (vacuolar) membrane dynamics. The cytoplasm was degraded by direct enfolding of lysosomes or vacuolar restrictive membranes(Sahu et al., 2011; Santambrogio et al., 2011), without the formation of autophagy vesicle structure.

Chaperon-mediated autophagy (CMA) indicates that lysosomal degradation of cellular organelles is selective. CMA can selectively degrade proteins containing KFERQ by identifying heat shot cognate 70 (Hsc70). Finally, the substrate-chapel-complex binds to the lysosomal associated type 2A membrane protein (LAMP2A)(Klionsky, 2007).

1.10 The importance of autophagy for cell survival

Autophagy works at low levels under physiological conditions to eliminate damaged organelles (such as mitochondria) and large molecules (such as proteins) to maintain normal physiological cell functions. In some cases, such as nutritional depletion, growth factor deficiency and ischemic hypoxia can upregulate autophagy. Cells can degrade certain components to release free amino acids and fatty acids, thereby

maintaining cellular ATP production and macromolecular synthesis. Due to the important role of autophagy in eliminating damaged mitochondria and other damaged organelles, the weakening of autophagy activity will result in the accumulation of damaged organelles and molecules in the cells, resulting in cell death (Brunk et al., 2002).

Autophagy has been established as a cell protecting mechanisms in adults stem cells of muscle (“satellite cells”), neuronal tissue (neuronal stem cells, NSC) and the blood-building system (hematopoietic stem cells, HSC). In hematopoietic stem cells a gradual reduction of autophagic flux was observed with increased cellular age, and in muscle satellite cells of elder donors a downregulated autophagy was associated with higher rate of cellular senescence and reduced capacity for self- renewal(L. Wang et al., 2019). In both cell types, mitochondrial dysfunction was seen in parallel to this age-related impairment of autophagy, leading to increased ROS production and shift in metabolic pathway towards oxidative phosphorylation(Leidal et al., 2018).

1.11 Autophagy as a pro-survival mechanism of cancer cells

The elucidation of the cellular signaling pathways involved in the regulation of autophagy revealed a close relationship between autophagy and the development and progression of malignant tumors(Zhang et al., 2015). Cancer cells were generally characterized by lower autophagy activity compared to healthy cells. Autophagy involvement in the elimination of malignant cells is suggested by its involvement in reducing chromosomal instability, proliferation, and inflammation of tumor cells. On the other hand, in certain pathological conditions, autophagy can also be a tumor-promoting mechanism by enabling tumor cells to survive. Such a mechanism is particularly important in situations of cellular stress or therapeutic interventions (hypoxia, nutrient deficiency, chemotherapy). For example, autophagy can be induced in response to various cancer treatments, especially chemotherapy therapy. This response may prove to be a mechanism that enables cell survival or favors and exacerbates death induced by these treatments(Hu et al., 2012; Zou et al., 2012).

1.12 Autophagy in pathogenesis and etiology of degenerative diseases

A common feature of many neurodegenerative diseases is the accumulation of mutated or toxic proteins and their aggregation in the cytoplasm. These diseases are termed "proteinopathies" and include, in particular, Huntington's disease, Alzheimer's disease or Parkinson's disease(C. Wang et al., 2018).

Accumulating and incorrectly folded protein aggregates can form, for example, as a result of a decrease in proteasome activity. Their presence leads to an increase in this induced autophagy, which is effective enough in the early stages of the disease to ensure its elimination. In an advanced stage, however, induced autophagy is no longer sufficient, and protein inclusions are formed in the cells. Similar to the accumulation of dysfunctional lipids, such clumped protein inclusions can irreversibly damage the affected cells (in the described case, the neurons) and thus form the trigger for the neurodegenerative disease(Benito-Cuesta et al., 2017; X. Liu et al., 2015; Switon et al., 2017).

Secondary neuropathies are also one of the most frequent secondary complications affecting patients with diabetes mellitus. These diabetic polyneuropathies are a peripheral nerve disorder that occurs as a result of chronic hyperglycemia. It can affect both the deliberately controlled part of the peripheral nervous system (somatic nervous system) and the autonomous nervous system (e.g. regulation of breathing, heart rate, bowel movements)(Charnogursky et al., 2014). It is unclear, however, if these diabetic polyneuropathies are also related to an impaired autophagy in the affected neurons, resulting from chronic hyperglycemia or from cytotoxic stress of AGEP (advanced glycation end products).

Diabetic polyneuropathy affects only peripheral nerves, causing a general sensorimotor neuropathy. In the context of chronic foot ulceration in T2D patients, there is a general observation that sensory neuropathy precedes the cutaneous complication(Vincent et al., 2011). It is unclear, however, if this is just co-incidental, with a common underlying defect (for instance diabetic vasculopathy affecting the

microvasculature) that causes both the cutaneous and the senso-neuronal symptoms, or if the polyneuropathy is really causative for the wound healing complications.

Impairment of autophagy is also considered a major factor in the pathogenesis of osteoarthritis, reflecting the age related downregulation of autophagy in chondrocytes and the increase of risk for the disease in the third trimester of life. Key proteins that play an important role in autophagy were found to be gradually reduced both in human and mouse cartilage(Carames et al., 2010; Carames et al., 2012). Since healthy articular cartilage shows a constant activity of autophagy, any impairment of the latter can lead to death of chondrocytes and structural damage to the affected joints(Carames et al., 2015). Autophagy can therefore be considered a chondroprotective mechanism.

1.13 Role of autophagy in stem cell therapy

Autophagy plays an essential role in regulating proliferation, differentiation and maintenance of MSCs of different origin. A range of specialized proteins are involved in autophagy in MSCs. Mammalian microtubule associated protein light chain3 (1ightchain3, LC3) is a homologous protein of yeast ATG8, including LC3-I and LC3-II forms. LC3-II is the only protein found to locate in autophagosomes and on autophagosomal lysosomal membranes. Its content is proportional to the number of autophagosomes, and it is a specific indicator of autophagy (Y. K. Lee et al., 2016). In MSCs, a large amount of autophagy activation was confirmed with high frequencies during the conversion of LC3-I to LC3-II, and may be dependent on the anti-apoptotic protein(L. Oliver et al., 2011).Therefore, many studies have focused on the role of autophagy induced by various intracellular and extracellular stimuli in stem cell try to maintenance and survival(Molaei et al., 2015).

Hyperglycemia caused by diabetes and metabolic syndrome can lead to dysfunction of blood vessels and organs, which has become a major hazard to human health. BMSCs cultured in a high-glucose environment showed premature cell aging, and telomere changes. Autophagy has a protective effect on cells under stress, and activates through up-regulation of Beclin 1, ATG5 and ATG7 expression, as well as

increased LC3-II conversion. Studies have found that knocking out ATG causes accelerated cell senescence, while carcinogenic stress induces stem cell senescence by activating autophagy(Capasso et al., 2015; Madeo et al., 2015). As cells senescent, they become bigger and flatter in shape, and eventually cease division. Meanwhile, the characteristics of stem cells are lost, thus affecting the clinical application of stem cells. Other studies have shown that MSCs of umbilical cord may accelerate wound healing in diabetic patients by increasing autophagy of damaged cells(Han et al., 2015). Autophagy is a kind of stress adaptation response, which can avoid cell death and inhibit cell apoptosis, and constitute an alternative path of cell death. Therefore, autophagy is also important to prevent cellular senescence, a process that can severely reduce stemness.

1.14 The relationship between autophagy, MSCs and radiation

Autophagy has been shown in somatic mammalian cells, (hepatocytes, cancer cells, cardiomyocytes), where it exerts a physiological function in recycling macromolecule precursors (amino acids, fatty acids) and providing ATP(Deretic et al., 2013; Kundu et al., 2008). Autophagy has also been shown at a low basal layer in cells of the embryonic inner-cell mass and embryonic stem cells. Upon differentiation, autophagy is upregulated, and a defect of it leads to a reduced formation of differentiating colonies(Tra et al., 2011; X. Zhou et al., 2011). The importance of autophagy in embryonic stem cells has been linked to their rapid proliferation during embryonic development and a high demand of macromolecular building blocks, and by the importance to clean the cells off difunctional organelles damaged by oxidative stress(L. Wang et al., 2019).

Mesenchymal stem cells, in contrast to embryonic stem cells are not rapidly proliferating, and neither do they exert a high metabolic rate. Since they normally reside in a protective stem cell niche, they are relatively safe from oxidative stress. It is therefore not clear, to which extent MSCs also rely on autophagy to provide of macromolecule precursors and ATP and to cleave organelles damaged by ROS.

MSCs during ex-vivo expansion and in a pre-differentiation state have been shown by us and by others(Bao et al., 2020; L. Oliver et al., 2012) to suffer from a gradual reduction of initial radiation response (Bao et al., 2020; L. Oliver et al., 2012).

Recent studies have found that reactive oxygen species (ROS) produced by cells after irradiation play a significant role in the occurrence and development of para-radiation effects. ROS considered being toxic byproducts of aerobic metabolism and the main cause of macromolecular damage. Excessive production of ROS causes changes in cellular environment and composition, such as lipids, proteins and DNA. The ROS produced by body in the aerobic pathway acts as a mutation inducer. The guanine on the DNA strand can be oxidized to 8-hydroxyguanine (8-OHdG). During DNA replication, 8-OHdG is prone to mismatch with adenine, resulting in G:C to T:A mutation and DNA damage(D. Wang et al., 1998). In addition, ROS can cause other forms of DNA damage, including DNA strand breaks, DNA site mutations, DNA double-strand aberrations. At the same time, DNA damage may also aggravate ROS and oxidative stress processes. For example, DNA damage can induce ROS production through the H2AX - reduced coenzyme II oxidase 1 (Nox1)/Rac1 pathway(Kang et al., 2012). If DNA damage is not repaired in time, the accumulation of DNA damage will activate the aging process and induce age-related diseases. In addition, mutations in DNA repair genes can affect the biosynthesis of proteins, thereby weakening their repair functions (I. Shimizu et al., 2014).

In particular the DNA damage response pathway (DDR), mediated by ATM, DNA-PK, gH2AX and 53BP1 is efficiently induced by IR in early passage MSCs, but suffers from reduced activity in aged hMSCs(Hladik et al., 2019). A radiation-induced autophagy could therefore also be impaired as a result of down-regulated DNA damage response.

The first goal of my study was to validate the human MSCs as a model to study autophagy. For this, I used the immortalized L87 cell line. As an inducer of autophagy, oxidative stress is (beneath starvation) a strong agent. Ionizing radiation-induced ROS

has been demonstrated in yeast cells and in human tumor cells to efficiently trigger autophagy(Jo et al., 2015; T. G. Lee et al., 2020).

1.15 Oxidative stress and covalent changes in proteins and lipids

When body is in a pathological state, too much highly active molecules in the body such as active oxygen free radicals (ROS), the degree of oxidation will exceed the scavenging ability of the oxide, and the oxidation system and anti-oxidation system will be unbalanced, resulting in tissue damage(Bizzozero et al., 2009). When ROS reaction activity is too high, it can quickly react with various biological macromolecules in the cell, causing damage at the cellular level, including oxidative damage to DNA, lipids and proteins(Dalle-Donne et al., 2003). Proteins play important roles in catalysis, regulation, transport, storage, in normal life activities of organisms. Therefore, some scholars believe that oxidative damage of proteins plays a crucial role in the pathophysiology of diseases(Fernandez-Checa et al., 2010).

Protein carbonylation is a type of protein oxidative damage, which itself is an irreversible chemical modification in oxidative stress(Zheng et al., 2010). Modification of protein carbonylation will cause changes in protein structure, so that it loses its original biological function. Eventually leads to dysfunction of cells and tissues, and pathological and physiological changes in the body. Studies have shown that protein carbonylation is involved in aging, apoptosis, and the etiology and pathophysiology of various neurodegenerative diseases(Bizzozero et al., 2005; C. N. Oliver et al., 1987).

1.16 Autophagy as an intracellular detox mechanism and the link to lipid droplets

Autophagy is an important pathway of lipid metabolism (Singh et al., 2009). The lysosomal pathway of autophagy increases LD decomposition in cells. Lipids can bind to other cellular components or be isolated in autophagosomes as a unique cargo. After that, autophagolysomes are formed, which are composed of autophagosomes

and lysosomes， then lipid-droplets breakdown(Mizushima et al., 2007). The degradation products of LD decomposition, such as free fatty acids (FFA), are released into the cytoplasm. FFA can maintain the rate of mitochondrial β-oxidation to generate ATP to maintain cell energy homeostasis. Mitochondrial β-oxidation is impaired by the reduction of FFA from LD decomposition(Finn et al., 2006)(Figure 4).

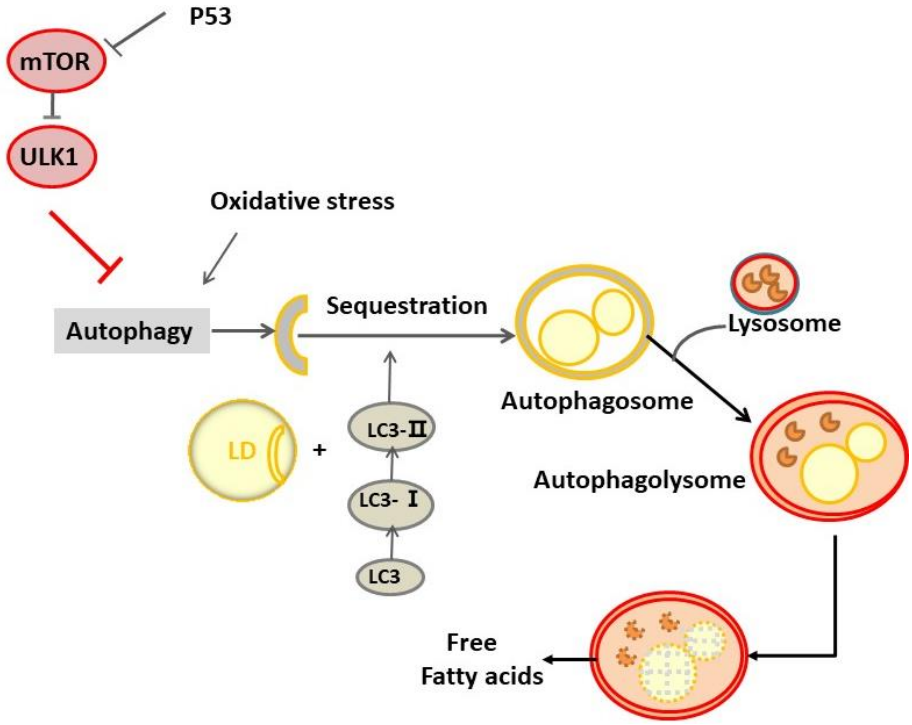

Figure 4: Regulation of lipophagy.

Initially, lipophagy was most intensively studied in hepatocytes because its role in the prevention of liver steatosis. Under the influence of inhibitions of autophagy genes or drugs, triglycerides (TG) content and the size of LD in cells would be affected(Sanyal et al., 2001). This can be explained by drug-induced mitochondrial toxicity with increased ROS production. Patients taking these drugs are detected with elevated levels of liver TG(Stankov et al., 2012).

Autophagy can remove lipid droplets accumulated in hepatocytes, which reduce lipid toxicity and improve their insulin sensitivity(S. W. Zhou et al., 2014). It was confirmed that in transgenic animal models induced by high-fat diet, autophagy levels in hepatocytes of obese and insulin-resistant mice were significantly reduced. In liver specific ubiquitin-like modified activating enzyme (ATG7) knockout mice, liver fat

deposition increased significantly. After repromoting the expression of ATG7, the expression levels of becn-1, ATG5, ATG1 2 and LC3 increased significantly. In addition, autophagy level also increased, and insulin resistance and glucose tolerance were significantly improved(Mizushima et al., 2011).

1.17 Formation and decomposition of lipid droplets

As organelles are for storing energy and metabolizing fatty acids and sterols, lipid droplets are responsible for the synthesis of numerous membrane structures and hormones(Hashemi et al., 2015)

Cells can also process excess lipids by esterifying potentially toxic lipids to form inert neutral lipids (such as triacylglycerol or sterol esters) (Yu et al., 2017). Lipid droplets play a key role in the regulation of intracellular lipid metabolism. Excessive expansion of lipid droplets will lead to lipid metabolism disorder, which is one of the most important characteristics of insulin resistance, type 2 diabetes, non-alcoholic fatty liver disease and other diseases

Lipid droplets compose of a single phospholipid layer, ranging in a size of diameter < 1–100μm, which surrounds hydrophobic triglycerides. Within the phospholipid monolayer some distinct surface proteins are embedded such as diacylglycerol O-acyltransferase 2 (DGAT2), Rab18, perilipin.

There are three processes involved in the formation of lipid droplets (Figure 5)：
(1) Synthesis of neutral lipids and formation of oil lens
(2) Lipid droplet budding from the membrane bilayer and fusion

(3) Lipid droplets expanding and growth.

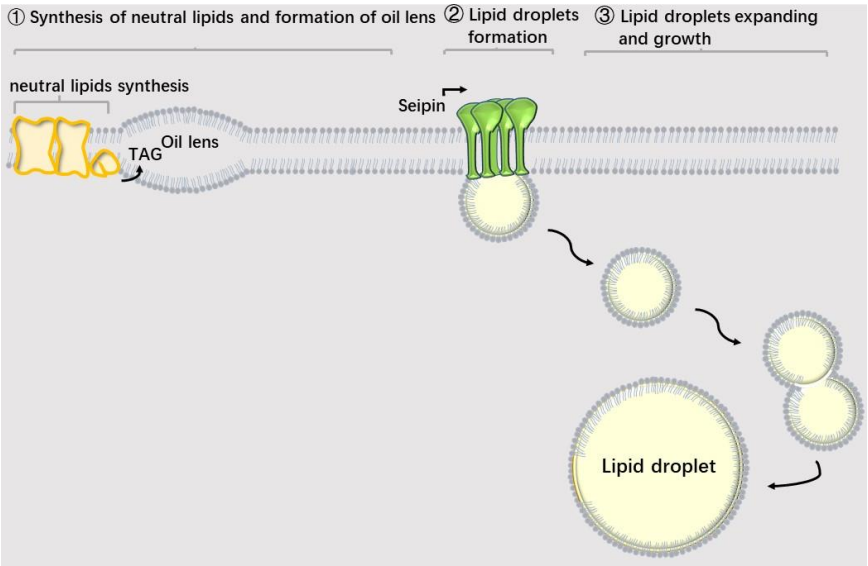

Figure 5: Steps in lipid drops formation.

The formation of the oil lenses always takes place within the phospholipid bilayers, as they exist in the cell membrane, the ER, golgi or mitochondria. There, neutral lipids aggregate between the lipophilic tails of the membrane phospholipid bilayer. As their concentration increases, neutral lipids are dispersed from the endoplasmic reticulum and gathered to form an oil lens. Consistently, no proteins are directly involved in lens formation and it is unclear whether there are preferential sites in the membrane bilayer for their formation(Olzmann et al., 2019).

In the second step, in the lens of neutral lipids, lipid droplets bud from the endoplasmic reticulum (ER) membrane due to differences in the surface tension of endoplasmic reticulum. In vitro experiments, membrane tension affects budding efficiency and also exerts directionality during the budding process. Due to the asymmetric recruitment and the binding of phospholipids and protein components, surface tension differences in the endoplasmic reticulum luminal leaflets ultimately determine the budding directionality(Chorlay et al., 2018). Seipin is a 2-fold transmembrane endoplasmic reticulum intrinsic protein, which is highly expressed in adipose tissue, and nervous system(Lundin et al., 2006). One function of Seipin is to regulate the size and morphology of lipid droplets, which is essential in the assembly and morphology maintenance of lipid droplets(Sim et al., 2014). In cells, fat

storage-inducing transmembrane (FIT) proteins promote lipid droplet induction. The lack of FIT proteins in mammalian cells inhibits the budding of lipid droplets (Gross et al., 2011; Hayes et al., 2017).

The third step, lipid droplets expand and grow. Lipid droplets then expand by droplet-droplet fusion.

COP-I protein promotes the budding of small lipid droplets and can reduce the phospholipid component of membrane on the surface of lipid droplets, thus increasing the surface tension of lipid droplets and facilitating the fusion with other membrane structures(Pol et al., 2014; Wilfling et al., 2014).

1.18 Decomposition of lipid droplets

LDs are dynamic structures within the cell, and unlike essential organelles such as mitochondria, ribosomes, golgi etc., LDs can also be degraded in the cells under certain circumstances.

(1) Lipid droplets are degraded by surface proteins

According to current studies, the degradation of LD can be mediated by proteins which bound to its surface. As is shown in Figure 6, These surface proteins include PAT protein family (perilipin, ADRP/adipophilin, Tip47 and related proteins) and Rab family(Robenek et al., 2005). Increasing of perilipin can reduce triglyceride hydrolysis and add its storage. Perilipin phosphorylated during fat decomposition promotes triglyceride hydrolysis. Moreover, the protein is necessary for transfer of hormone-sensitive lipases from cytoplasm to lipid droplets(Brasaemle et al., 1997).

(2) LDs are degraded by autophagy

When intracellular nutrients are scarce, autophagy is activated to provide substrates and raw materials for cellular metabolism. Autophagy is involved in maintaining the stability of the intracellular environment, controlling the metabolism and renewal of mitochondria and endoplasmic reticulum(Y. C. Kim et al., 2015). Autophagosomes isolate large lipid droplets or may consume small lipid droplets completely and send

them to lysosomes(Singh et al., 2009). Lysosomal acid lipase degrades triglyceride to fatty acid and glycerol

(3) Lipid droplets degraded by lipase

Adipose differentiation-related protein (ADRP) promotes the accumulation of neutral lipid droplets by inhibiting intracellular lipase. However, the mechanism of ADRP preventing lipase from localizing lipid droplets is still unclear(Imamura et al., 2002). Cytoplasmic lipase mobilizes lipid droplets under a series of catalysis included triglyceridase, hormone-sensitive lipase. 1 molecule of triglyceride is decomposed into three molecules of fatty acid and one molecule of glycerol(Zimmermann et al., 2004).

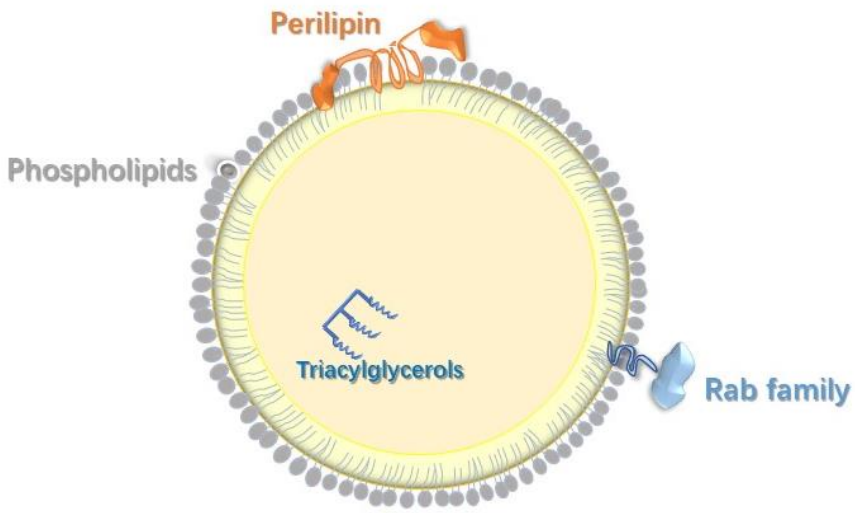

Figure 6: The structure and composition of lipid droplets.

1.19 Aim of this study

This thesis explores the difference between T2D patients derived bone marrow stem cells and healthy donor derived bone marrow stem cells, by using radiation as a stable condition to induce autophagy.

For a better understanding of the basic mechanisms of radiation-induced autophagy and formation of lipid droplets in mesenchymal stem cells, I used an immortalized human MSC cell line (L87). This cell line was also important to establish a γ-radiation dose response for LDs and autophagy, and to investigate the difference between acute and fractionated dose exposure. We used a low dose, fractionated X-irradiation, which is a known inducer of oxidative stress, to trigger autophagy in a very reproducible manner.

The X-radiation conditions that efficiently trigger autophagy and eliminate lipid droplets was than applied to a set of primary BM-MSCs derived from 4 healthy donors and from 4 T2D patients. I compared in these cells the baseline level of autophagy signaling proteins LC3-II as well as the response to low and to high X-ray dose challenges. The formation and elimination of lipid droplets was quantified as an autophagy end-point, reflecting the proficiency or deficiency of a cell to trigger autophagy after cellular stress.

We hoped to provide a new idea for autologous stem cell therapy. We believed that with the continuous understanding of these problems in the studies of tissue engineering, cell engineering and genetic engineering, the application of BMSCs in the clinical treatment of diabetic foot would become more feasible.

2. Materials and Methods

2.1 Materials and software

2.1.1 Chemicals and Reagents

Component	Company
Bovine Serum Albumin (BSA)	Sigma-Aldrich, Taufkirchen, Germany
DMSO	Merck, Darmstadt
dNTP	Thermo Fisher Scientific, Darmstadt, Germany
DTT 0.1 M	Thermo Fisher Scientific, Darmstadt, Germany
Ethanol (70%)	Merck, Darmstadt
Fetal bovine serum (Hyclone)	Thermo Fischer Scientific
Glycine	Roth, Karlsruhe
Hematoxylin	Sigma-Aldrich, Taufkirchen, Germany
Histo Fix (4% PFA)	AppliChem GmbH, Darmstadt, Germany
Hoechst 33342 (Hoechst)	Thermo Fisher Scientific, Darmstadt, Germany
Isopropanol	Merck, Darmstadt, Germany
Methanol (100%)	Merck, Darmstadt, Germany
$MgCl_2$	AppliChem GmbH, Darmstadt, Germany
NaCl Sodium chloride)	AppliChem GmbH, Darmstadt, Germany
Nonfat Dry Milk powder	Sigma-Aldrich, Taufkirchen, Germany
Oil red O	Sigma-Aldrich, Taufkirchen, Germany
Oligo(dT)12-18 primer	Thermo Fisher Scientific, Darmstadt, Germany
Penicillin / Streptomycin	Biochrom GmbH, Berlin, Germany
Potassium hexacyanoferrate II	Sigma-Aldrich, Taufkirchen, Germany

Potassium hexacyanoferrate III	Sigma-Aldrich, Taufkirchen, Germany
Power SYBR™ Green PCR Master Mix	Thermo Fisher Scientific, Darmstadt, Germany
Propidium iodide	Thermo Fisher Scientific, Darmstadt, Germany
Protease Inhibitor Cocktail	Roche, Germany
Proteinase K	Roche Diagnostics, Basel, Switzerland
RNAaseOUT (40 units/µL)	Thermo Fisher Scientific, Darmstadt, Germany
SuperScript II RT	Thermo Fisher Scientific, Darmstadt, Germany
Triton-X-100	Sigma-Aldrich, Taufkirchen, Germany
Trypsin-EDTA 0.05%	GibcoTM Thermo Fisher Scientific, Darmstadt, Germany
X-gal	Thermo Fisher Scientific, Darmstadt, Germany

2.1.2 Buffers and solutions

Buffers and solutions	**Content**	
Oil Red O Staining		
Oil Red O stock solution	Oil Red O	300 mg
	Isopropanol	100 mL
Oil Red O working solution	Oil Red O stock solution	60%
	distilled water	40 %
CHH labeling		
CHH solution	1 x PBS	

	7-(Diethylamino)-coumarin-3-carbohydrazide	
	0.02 mmol/L	
Blocking Solution CHH labeling	1 x PBS	
	FBS	5%
	Tween-20	0.1%
Immunofluorescence		
PBS + (γH2AX)	1 x PBS	100mL
Blocking Buffer	BSA	1%
Antibody Dilution Buffer	Glycin	0.15 g
LC3B	1 x PBS	
Blocking Buffer	BSA	5%
	Triton X-100	3%
Western Blot		
Blocking Buffer	1 x TBST	
	w/v non-fat dry milk	8%
Lämmli Sample Buffer (4x)	SDS	2%
	Glycerol	6%
	B-mercaptoethanol	150 mM
	bromophenol blue	0.02%
	Tris–HCl	62.5 mM
	Supplied at pH 6.8	
Primary antibody dilution buffer	1 x TBST	
	BSA	5%
RIPA Buffer	Tris HCl NaCl NP-40	pH 7.6 25mM 150mM

	sodium deoxycholate SDS Protease Inhibitor complete Mini (Roche)	1% 1% 0.1%
1 x PBS	Na^+ Cl^- K^+ HPO_4^{2-} $H_2PO_4^-$	57 mM 140mM 4.45mM 10.1 mM 1.76 mM
1x Tris Buffered Saline (TBS)	Sodium Chloride Tris. Supplied at pH 7.6	137 mM 20 mM
10 x Tris buffered saline with Tween-20 (TBST)	Sodium Chloride Tris Tween®20 Supplied at pH 7.6	137 mM 20 mM 0.1%
10x Tris Glycine SDS Running Buffer	Tris Glycine SDS Supplied at pH 8.3	25 mM 192 mM 0.1%
10x Tris Glycine Transfer Buffer	Tris Glycine Methanol Supplied at pH 8.3	25 mM 192 mM 20%
Senescence staining		
Senescence staining solution	X-gal senescence assay buffer solution	100 µg 5 ml
Senescence assay buffer solution	Di-Sodiumhydrogen phosphate dihydrate	1.42 g

	MgCl2	81.32 mg
	NaCl	1.75 g
	Potassium hexacyanoferrat II	400 mg
	Potassium hexacyanoferrat III	320 mg
	aqua dest.	200 ml
	Citric acid Adjust to pH 6	

2.1.3 Medium

Cell culture medium
DMEM/ F-12 (1x) (+ GlutaMAX^{TM}) (Thermo Fisher Scientific)
αMEM(1 x) (+ GlutaMAX^{TM})(Thermo Fisher Scientific)
DMEM (1 x) (+ GlutaMAX^{TM}) (Thermo Fisher Scientific)
RPMI1640 (1 x) (+ GlutaMAX^{TM}) (Thermo Fisher Scientific)
Stem MACS (Miltenyi Biotech)

2.1.4 Cell lines

L87 (Kind gift from Prof. P. Nelson, LMU Department of internal medicine and nephrology)

Human BMSCs (kindly provided by Dr. Schoenitzer, Department of Surgery, Experimental Surgery, and Regenerative Medicine, Ludwig-Maximilians-University Munich)

Human adipose derived mesenchymal stem cells (hADMSC) (provided by Dr. Duscher, Department of plastic and hand surgery, Klinikum rechts der Isar, Technical University of Munich)

2.1.5 Supplements

Supplements	Company
Human FGF-2	Miltenyl Biotec, Germany

2.1.6 Donors Number

No.	Gender	Age
Healthy Donors		
H-7	Male	60
H-19	Male	49
H-33	Male	46
H-44	Male	44
Type two diabetes		
T2D-14	Male	45
T2D-42	Male	46
T2D-60	Male	68
T2D-62	Male	56

2.1.7 Antibodies used in the experiment and their usage

Antibody	Species of antibodies	Dilution	Company
Anti-γH2AX monoclonal	Mouse	1:500	Millipore, Schwalbach, Cat # 05-636
Cy3-conjugated anti mouse	Sheep	1:500	Jackson Immunoresearch, West Grove (USA), No. 515165-003
Anti-LC3B polyclonal	Rabbit	1:1000 1:200	Cell signaling technology, # 2775
Anti-Rabbit IgG (H+L), F(ab´)$_2$ Fragment, Alexa Fluor 488 Conjugate	Goat	1:1000	Thermo Fisher Scientific, Cat # A32731
Anti-Rabbit IgG, HRP-linked Antibody	Goat	1:1000	Cell signaling technology, Germany Cat # 7074
Anti-beta Actin	Mouse	1: 500	Sigma, Germany #A2228
Anti-mouse IgG, HRP-linked Antibody	Horse	1:1000	Cell signaling technology, Germany #7076

2.1.8 Real-Time PCR

List of primers used for real-time PCR

Gene	Forward primer	Reverse primer
hGADPH	5'-AGAAGGCTGGGGCTCATTTG-3´	5´-AGGGGCCATCCACAGTCTTC-3´
hPPARg	5'- AGAAGCCTGCATTTCTGCAT-3'	5'-TCAAAGGAGTGGGAGTGGTC-3'
hPRDM16	5'-CCAGTGAGAAGCAGGAGGAC-3'	5'-CGGCTCCAAAGCTAACAGAC-3'

2.1.9 Consumables

Product	Manufacturer
Cell culture flasks (T25)	Greiner, Frickenhausen, Germany
Cover slips (24 x 50 mm)	VWR, Darmstadt
Cryo tubes, 2ml	Steinfurt, Germany
Falcon tubes (50 ml, 15 ml)	Greiner, Frickenhausen
Microscope slide	Thermo Fischer Scientific, Frankfurt am Main
Millex GP filters (0.22 µm)	VWR, Darmstadt
Multiwell plates (6-/12-/24-/96-well)	Sigma Aldrich, Steinheim
Pipette Tips	StarLab, Ahrensburg
Plastic pipettes (5-/10-/25-/50 ml)	StarLab, Ahrensburg

2.1.10 Equipment

Device	Manufacturer
Centrifuge Sigma 3K15	SIGMA Laborzentrifugen GmbH, Osterode am Harz, Germany
Heating block Thermomixer compact	Eppendorf, Hamburg, Germany
Incubator 37 °C, 5% CO_2 for cell culture	Heraeus Holding GmbH, Hanau, Germany
Inverted microscope Olympus CK2	OLYMPUS EUROPA SE & CO. KG, Hamburg, Germany
Magnetic stirrer	IKA-Werke GmbH & Co. KG, Staufen, Germany
Microscope Axiovert 25	Carl Zeiss, Jena, Germany
Microscope KEYENCE BZ-9000 series	KEYENCE Deutschland GmbH, Neu-Isenburg, Germany

pH meter Lab850	SI Analytics GmbH, Mainz, Germany
Pipettes 2, 10, 20, 100, 200, 1000 µl	Gilson, Inc, Limburg, Germany
StepOnePlus Real-Time PCR System	Applied Biosystems, Darmstadt, Germany
X Strahl RS225 X-ray source	Surrey, UK
Z Series Coulter Counter - Z1	Beckman Coulter GmbH, Krefeld, Germany

2.1.11 Software

Software	Company
AxioVisionAC 4.2	Carl Zeiss, Germany
Photoshop CS6	Adobe
BZ-II-Analyzer	Keyence
Prism 7	GraphPad
ImageJ	Open Source
StepOne software v2.3	Applied Biosystems, Germany

2.1.12 Commercial kits

Kit	Content	Company
Maxwell 16 miRNA Tissue Kit	Homogenization Solution Lysis Buffer 1-Thiolycerol DNase I Blue Dye Maxwell RSC Cartridges Maxwell RSC Plunger Pack Elution tubes, 0.5 ml Nuclease-free water	Promega, Madison, USA
Pierce BCA Protein Assay Kit	BCA Reagent A BCA Reagent B Albumin Standard Ampules	Thermo Fisher Scientific

2.2 Methods

2.2.1 Ethics statement

The study has been approved by the Ludwig-Maximilians-University review board (project number: 238/15) and all donors have obtained written informed consent before participating in the study. All of the donors were screened as healthy or type 2 diabetes (T2D). This study focused on eight males, including four healthy and four T2D, with a mean age of 51.8 years (range, 44–68 years).

The Human adipose derived mesenchymal stem cells (hADMSCs) were from company: Lonza, donor 29635, catalog#: LO PT-5006.

2.2.2 Cell Culture

2.2.2.1 Extraction of primary Human BMSCs

The L87 cell line was provided by Prof. P. Nelson, LMU Department of internal medicine and nephrology as a gift. It has been established from a donor BM-MSCs after immortalization with the SV40 large T-antigen. It has been shown express MSC markers and cell characteristics for at least 100 cell generations(Thalmeier et al., 2001).

The Human adipose derived mesenchymal stem cells (hADMSCs) were cultured in StemMACS medium. hADMSCs were cultured in vitro and spontaneous differentiated into preadipocytes for later experiments.

Human primary BM-MSCs (T2D-MSCs (n=4), healthy-MSCs (n=4)) were collected from Department of Surgery, Experimental Surgery, and Regenerative Medicine, Ludwig-Maximilians-University Munich. Human MSCs were isolated from femoral head fracture patients during replacement surgery. Samples were collected in anticoagulant tubes and stored at 4 °C.

2.2.2.2 BMSCs cultivation

(1) Bone grafts obtained from surgery were washed with PBS three times.

(2) Bone grafts then incubated in DMEM medium containing 250 U/ml collagenase II at 37 °C three times for 10 min.

(3) 100 μm cell strainers were used to filter bone marrow diluent.

(4) Bone marrow diluent was centrifuged at 500×g for 5 min.

(5) The cells were plated in T25 cell culture flasks, filled with 5ml αMEM (Thermo Fisher Scientific) medium, 10% fetal bovine serum (FBS) and 1% penicillin/streptomycin. The medium was changed every 48 h. BMSCs were obtained by removing the non-BMSCs according to their adhesion ability.

2.2.2.3 Culturing of primary MSCs

(1) After 70% to 80% of primary BMSCs were confluency, culture medium was discarded. Cells precipitate was collected, washed twice with PBS, and 0.05% trypsin was added at room temperature.

(2) Cells were incubated in humidifying incubator at 5% CO_2 and 37 °C for 5 min. Cells digestion were observed under the microscope. After the digestion was completed, 10% FBS medium was added to terminate trypsin digestion, and straw was gently blown for several times.

(3) Cells suspension was transferred to a 15 mL sterile centrifuge tube, centrifuged for 5 min. Cells precipitate was collected, washed twice with 1×PBS, and then added to culture medium for further culture.

(4) Cells were passaged by subculture at a ratio of 1:3.

(5) Plastic adherent cells were selected from 4-6 passages in vitro. These cells were cultured in DMEM/F-12+GlutaMAX medium with 10% FBS. hADMSCs were cultured in Stem MACS.

(6) 10ng/mL Human FGF-2 was warmed up in 37 °C. Human FGF-2 was added at each time when changing medium to avoid senescence. For senescence staining,

medium was changed to normal medium without Human FGF-2 before radiation. Medium was changed every 3-4 days and cells were passaged every three days.

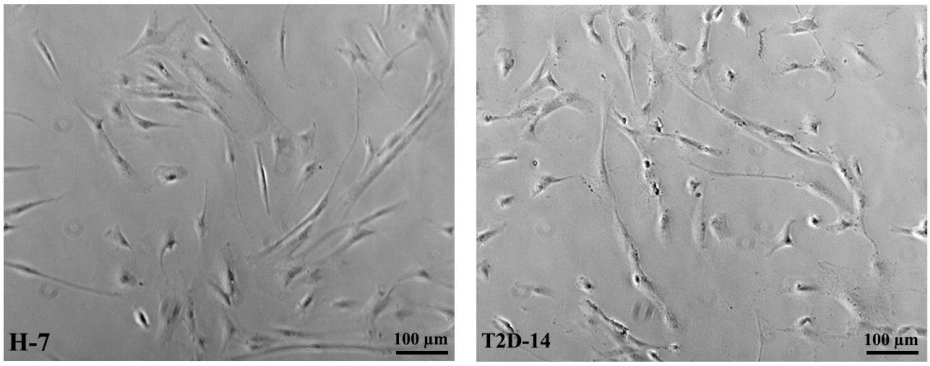

Figure 7: Representative images of human mesenchymal stem cells (MSCs).

H-7 represented healthy donors, and T2D-14 represented type 2 diabetes donors.

2.2.2.4 MSC cryopreservation

(1) The frozen culture medium was prepared containing 10% DMSO and 10% FBS.

(2) After 70% to 80% of BMSCs were confluency, monolayer of cells was digested with trypsin. Suspended cells were transferred directly to a 15 mL centrifuge tube.

(3) Centrifuge at 1,000 rpm for 5 min

(4) Trypsin and old culture medium were removed, and an appropriate amount of the prepared frozen culture medium was added. The cells were then gently blown with a straw to make them evenly. The final cell density in the frozen medium was adjusted to 2×10^6/ml ~ 3×10^6/ml.

(5) Cells were divided into cryopreservation tubes (1 ~ 1.5 ml each).

(6) Label cryopreservation tube with cell name, cryopreservation time and operator.

(7) Freeze-storage: the standard freeze-storage procedure was the cooling rate of -1 ~ -2 °C / min, then put it into the refrigerator at -80 °C overnight. Take out the freeze-storage tube and transfer it into the liquid nitrogen container.

2.2.2.5 MSC thawing

(1) Remove freezer tube from the liquid nitrogen container and immerse it in warm water at 37 °C.

(2) Remove cryopreservation tube from 37 ℃ water bath, open the lid, suck out cell suspension with a straw, add it to centrifuge tube and vortex the medium more than 10 times to mix well.

(3) Centrifugation at 1,000 rpm, 5 min.

(4) Discard supernatant, add culture medium containing 10% FBS to resuspend cells, count, adjust cell density, culture stand in humidifying incubator at 5% CO_2 and 37 ℃.

(5) The next day, medium was replaced and cultured continuously.

2.2.3 X-Irradiation

Cells were exposed to 195 kV X-rays at a dose rate of 0.813 Gy/min (10 mA, Al filter) using the X-Strahl RS225 source. Throughout radiation, cells were maintained in closed cabinet X-ray chamber at room temperature (Figure 8). Cells were returned to normal growth conditions immediately after radiation and maintained for various periods of time before fixation.

The radiation dosages were chosen for L87 to induce autophagy by various doses of radiation (0.03 Gy; 0.21 Gy; 3 Gy). The radiation experiment with the L87 cells was conducted in 6 different dose groups (control; 0.03 Gy; 0.03 Gy/ No FBS; 0.21 Gy; 6 ×0.03 Gy / 3 Gy; 7×0.03 Gy). The experiments with the multiple irradiation (7× 0.03 Gy) were conducted over a period of 4 days, with 6 and 18 hours intervals between the individual X-ray fractions. Cells were incubated at 37 ℃ for 18h after radiation to obtain autophagy.

We used different doses (0.03 Gy, 3 Gy) to investigate the relationship between X-irradiation, autophagy and the formation of lipid droplets.

Figure 8: X Strahl RS225 radiation machine as used in the Research Unit Medical Radiation Physics and Diagnostics at Helmholtz Center Munich.

2.2.4 RNA isolation and reverse transcription

(1) RNA was isolated using the Maxwell 16 miRNA tissue kit. For RNA isolation, the reaction mixture was added following the instructions. T25 flasks were put on ice for 10 min, then cells were scratched, and the lysate collected. This lysate was transferred to Maxwell RSC Cartridge.

(2) the DNase I Solution was prepared by adding 275 µL nuclease free water to the lyophilized DNase I. For visual aid for pipetting 5 µL of a blue dye was added. From this solution 10 µl was transferred to each cartridge.

For final preparation of the cartridges one plunger and elution tubes with 60 µL nuclease free water was placed in the appropriate position. The cartridges were now ready to use, and the RNA was extracted using Maxwell RSC 16 Instrument.

The concentration and purity of RNA were measured by absorbance method with Tecan Infinite M200 microplate. 1 µL from each sample were added on Nano Quant plate. Nucleic acids absorb light most actively at 260 nm. An A260/A280 ratio between 1.8-2.0 is considered as pure nucleic acid. Higher or lower ratios may indicate the presence of contaminants such as proteins, which absorb at 280 nm.

To generate cDNA for quantification by qRT-PCR, the RNA was reverse-transcribed using SuperScript® II Reverse Transcriptase (Thermo Fisher Scientific, Germany).

(1) Mixture was added in the following Table 1.

Table 1: Reaction mixture for reverse transcription

Reagent	Quantity (µL)
Oligo dT (0.5 µg/µl)	0.5
Random primers (50-250 ng)	0.5
250ng mRNA	
dNTPs (10 mM)	1
Distilled water	To 12

(2) The mixture mixed gently up and down, incubate at 65 °C for 5 min

(3) Mixture was added in the following Table 2, incubate at 42 °C for 2 min.

(4) Afterwards, 4 µL 5X First-Strand Buffer, 2 µL 0.1M DTT and 1 µL RNaseOUT (40 units/µL) were added, mixed and incubated for 2 min at 42 °C.

(5) Add 1µL of SuperScript® II Reverse Transcriptase. The mixture mixed gently up and down, incubate for 50min at 42 °C.

(6) Inactivation and denaturation were reaction at 70 °C for 15 min

(7) cDNA stored at -20 °C or continue do Real-time PCR immediately.

SYBR-Green Master Mix (PowerUp, Thermo Fisher Scientific, Germany) was used for quantitative real-time PCR according to the manufacturers protocol. For running Real-Time PCR, a reaction mixture was prepared as following Table 3:

Table 2: Reaction mixture for real-time PCR

Reagent	Quantity (µL)
Power SYBR™ Green PCR Master Mix	10
Primer mixture [forward primer (5pmol/µl) and reverse primer (5pmol/µl)]	1
Nuclease free water	6
cDNA	3

The solution was mixed at the bottom of 96 well plate and centrifuged at 1000rpm for 3 min. The prepared 96-well plate was sealed with transparent foil and placed on the StepOnePlus Real-Time PCR System for PCR amplification. The reaction conditions are as follows.

Table 3: Real time PCR running method.

Steps	Temperature (°C)	Time
Holding stage (initial denaturation)	50 95	2 min 2 min
Cycling stages I 40x (denaturation)	95	15 sec
Cycling stage II 40 x (annealing and elongation)	60	1 min
Melt curve stage I	96	15 sec
Melt curve stage II	60	1 min
Melt curve stage III	95	15 sec

40x cycles were repeated for amplification of cDNA. The human GADPH gene acted as the housekeeping gene. For quantification, the comparative CT method was employed. Where CT stands for cycle threshold and the ΔCT (sample) is the CT value of any sample normalized (subtracted from) to the house keeping gene, while ΔCT (reference) is the CT value for the control samples also normalized (subtracted from) to the house keeping gene. Afterwards, ΔΔCT was calculated, which is the difference between the ΔCT values of treated samples subtracted from the control samples. A normalization step for target gene expressions which compensates for the fold changes during amplification was also carried out. The relative expression of RNA was determined using the $2^{-\Delta\Delta Cq}$ equation.

2.2.5 7-(Diethylamino)-coumarin-3-carbohydrazide (CHH) labeling of lipid carbonylation

(1) L87 cells were grown on 6-well culture plates. After different treatments, cells were washed (PBS, two times), fixed (4% PFA, 15 min, 37 ℃) and washed again (PBS, two times).

(2) For CHH labeling cells were blocked in blocking solution (5% FBS, 0.01% Tween-20 in PBS, 1h, 37 ℃) and incubated with CHH (0.02 mmol/L, 2h, 37 ℃).

(3) Afterwards, cells were washed 3 times with PBS and nuclei were counterstained with propidium iodide. The staining was observed under Keyence BZ 900 microscope. For quantification integrated density was measured using ImageJ.

2.2.6 Oil red O Staining

(1) After 24 h or 18 h radiation, the cells were washed with PBS three times, fixed for 10min with 4% PFA at room temperature and washed with sterile double distilled water three times.

(2) After filtering the oil red working solution twice through a syringe filters (0.22 μm), cells containing lipid droplets were stained for 45 min at room temperature with Oil red O solution (stock solution: 3 mg/ml isopropanol; Oil red O working solution: 60% Oil Red O stock solution and 40% distilled water). Isopropanol is highly volatile, resulting in the precipitation of solid oil red crystals. To avoid interference of the cell staining with those particles, the staining solution is not easy to preserve and should be reformulated each time. Working solution is stable for no longer than 2 h.

(3) After staining, cells were washed with sterile double distilled water and the nuclei were counter-stained with hematoxylin staining solution. Lipid droplets were observed under Axiovert 25 microscope. Images were acquired at 40x magnification and AxioVisionAC 4.2. The intensity was quantified by measuring integrated density using ImageJ.

2.2.7 Immunofluorescences staining

2.2.7.1 γH2AX

Immunofluorescent staining of γH2AX foci

(1) After 1.5 h radiation, cells were fixed on coverslips in 4% PFA for 15 min and permeabilized with 0.2% Triton-X100 in PBS.

(2) Nonspecific antibody binding was blocked by adding PBS^+ blocking solution (1% BSA, 0.15% Glycin, PBS) for 1 h. Cells were incubated with primary antibody against γH2AX (dilution 1:500) diluted in PBS^+ over night at 4 °C in a humidified box.

(3) After several rinses with PBS, cells were incubated for 1 h with Cy3-conjugated anti-mouse antibody (dilution 1:500) diluted in PBS^+. This procedure was carried out in the dark.

(4) Cells were counter-stained with Hoechst33342 and covered with water and cover slips. All procedures were carried out in the dark.

Quantification of γH2AX foci

(1) Images of stained cells were taken under 40x fold magnification and edited with haze reduction and black balance by the BZ-II Analyser software (Figure 9).

(2) For the analysis γH2AX foci, all slides of one experiment (treated and control cells) were visualized at the microscope within 12 h pictures by one person and analyzed at the same time (Figure 10). For each experiment, at least 100 cells were counted.

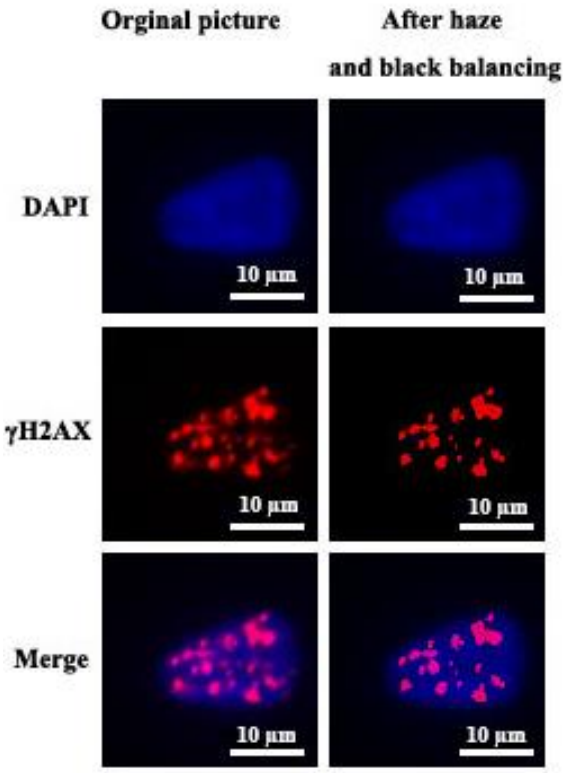

Figure 9: Representative images BMSCs after 3 Gy radiation.

Immunofluorescent stained γH2AX foci. Red color indicating cellular recognition of DNA double-strand breaks and their repair. Left pictures were the original ones taken by the Keyence microscope. Right pictures were edited by the Keyence analyzer software to reduce hazard and balance black backgrounds. The picture of the Hoechst-stained nuclei was merged with the γH2AX images in the bottom line. Scale bar: 10μm.

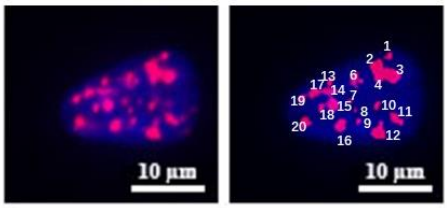

Figure 10: Quantification of γH2AX foci by researcher. In this example twenty foci were counted. Scale bar: 10 μm.

2.2.7.2 LC3B

(1) After 24 h or 18 h following X-irradiation, human-BMSCs on slides were washed

with PBS twice, and fixed with methanol at -20 ℃ for 20 min and blocked with blocking buffer (1X PBS / 5% BSA / 0.3% Triton™ X-100) 1 h at 37 ℃.

(2) The cells were incubated with the anti-LC3B antibody (1:200) in blocking buffer at 4 ℃ overnight.

(3) After washing the slides twice with PBS, they were incubated with an anti-rabbit secondary antibody (1:1000; Thermo Fisher Scientific) at 37 ℃ for 1 h.

(4) After washing the slides again twice with PBS, the cells were counter-stained with Hoechst 33342(10ng/mL) at room temperature for 5 min and covered with water and cover slips. All procedures were carried out in the dark. Visualization and image acquisition were done on a Keyence BZ9000 microscope using the fluorescence channels for GFP, Cy5 and DAPI and 40x plan fluor objective.

2.2.8 Western blot analysis

2.2.8.1 Preparation of SDS-PAGE gel

To separate the proteins, the samples were separated on a 12% polyacrylamide gel. The recipe for making a gel is listed in Table 5. Gels were poured into manufactured. Cassettes Briefly, all solutions for the separation gel were mixed in a 50 mL Falcon tube. TEMED and APS were added immediately before pouring the gel into the gel casting cassette. The cassette was loaded with 4.3 mL of the separation gel and the upper edge of the gel solution covered with 3 ml of iso-butanol. Polymerization was allowed to proceed for 30 minutes at room temperature. After removing the iso-butanol, a stacking gel was poured on top of solid separation gel. (The recipe is shown in Table 5.) A well-forming comb (1.5 mm 10-well) was inserted into the staking gel for the formation of sample bags. The polymerization was left in the room for 30 minutes.

Table 4: Components of 12% separating SDS-gel and a stacking gel

Components	Amount for 1 separating gels[mL]	Amount for 1 stacking gels[mL]
Acrylamide/Bis	2	0.3
H_2O	1.05	1.4
1 M Tris pH 8.8	1.9	
1 M Tris pH 6.8		0.25
10% SDS	0.05	0.02
10% APS	0.05	0.02
TEMED	0.005	0.002

2.2.8.2 Protein extraction and concentration measurement

For protein extractions from BM-MSC cells, cells were plated in T25 flasks with a concentration of 3 x 10^6 cells. Cells were washed twice with ice cold PBS and lysed directly on the cell culture vessel by adding 1 ml ice-cold lysis buffer (RIPA buffer, supplied with complete mini Protease Inhibitor Cocktail). Lysate on the flask surface was collected with a scraper and harvested in 1.5 ml Eppendorf tubes, kept on ice and sonicated. Before further analysis of the protein extracts were stored at -20 °C.

Protein concentrations were measured using the BCA protein assay kit using BSA (albumin standard) as the standard. The protein extracts were thawed on ice. For each sample to be analyzed 10µL of protein extract were mixed with 90µL water. For each standard curve a series of diluted BSA was prepared in the same way. To each sample or diluted BSA standard, 100µL of the BCA master mix was added. The vials were covered with parafilm to prevent evaporation from the reaction, mixed carefully and incubated at 60 °C in a water bath for 15 minutes, to carry out the colorimetric reaction. The resulting fluorochrome was measured as absorbance at 565 nm on a TECAN microplate reader. The standard curve was recorded in an Excel Program using a linear regression curve fit. The protein concentration of the cell extracts was

determined by finding the intersection between the measured 565nm absorption with the BSA standard curve.

2.2.8.3 Sample preparation, gel loading and PAGE electrophoresis

Protein extracts were thawed and kept on ice. The amount that equals 10 µg total protein for each sample was pipetted in a new tube and mixed with the equal volume of 2x Laemmli buffer (1: 1 ratio). After mixing by pipetting up and down, the tube was heated 5 minutes at 95 °C and quickly put on ice before loading on gels.

Gel casting cassettes with polymerized gels were inserted in the gel electrophoresis tank and the two buffer chambers filled with PAGE buffer. Protein molecular weight markers (7 µL) and up to 40 µL each sample was loaded into the wells of the gel using a fine pipette. The electrophoresis was carried out in two steps: a first run at 100 V for 10-15 minutes to Load proteins into the separation gel, followed by a voltage rise to 140-150 V for 1.5-2 hours to separate proteins. Electrophoresis was carried out at room temperature.

2.2.8.4 Protein transfer by blotting to nitrocellulose membrane

The separated proteins were transferred under moist conditions (tank transfer). Gels were taken of cast gel cassettes and rinsed with transfer buffer. A pre-wet nitrocellulose was placed directly on the gel, both were sandwiched between two pieces of blotting paper, two sponges, moistened (to ensure there are no air bubbles) and loaded into a compatible cassette. This "sandwich" was clamped together and placed in the transfer chamber filled with transfer buffer and a magnetic stirrer with the extinguishing membrane facing the positive charge. The transfer chamber was placed on a magnetic stirring plate in a box filled with ice. The transfer was 2 hours at 100V. After completion of the transfer, the separated proteins on the NC-membrane was detected and documented with a quick reversible Ponceau S staining. The membrane at this stage was either processed immediately with immunodetection, or left air-dried for later use.

2.2.8.5 Detection and quantification of the proteins

The membrane with transferred proteins was cut into pieces according to the size of the expected protein. These membrane pieces were placed in a box containing the blocking solution and incubated for 1 hour at 37 °C in a water bath with continuous shaking, followed by two rinses in T-TBS. Antibodies were diluted in 3% BSA / T-TBS in the indicated dilutions. The membranes were incubated with the antibodies overnight at 4 °C with continuous agitation on a rocking plate. Antibody incubation was followed by washing 2 times for 5 minutes in T-TBS under stirring conditions. HRP conjugated secondary antibodies were used according to the species of the first antibody, diluted 1:2000 in blocking buffer and used to incubate the membrane for 1 hour at room temperature. Excess or unpacifically bound secondary antibody was removed by shaking with T-TBS for 2 x 5 minutes. A commercially available Western blot chemiluminescence detection kit (Thermo Fisher Pierce, Life Sciences) was used to detect bound antibodies. The staining solution for detection was manufactured in accordance with the manufacturer's protocol. Western blot nitrocellulose membranes they were incubated in 4 mL of staining solution for 5 minutes at room temperature and the chemiluminescent signal was immediately visualized and recorded with the Alpha Innotech ChemiImager system (Figure 11).

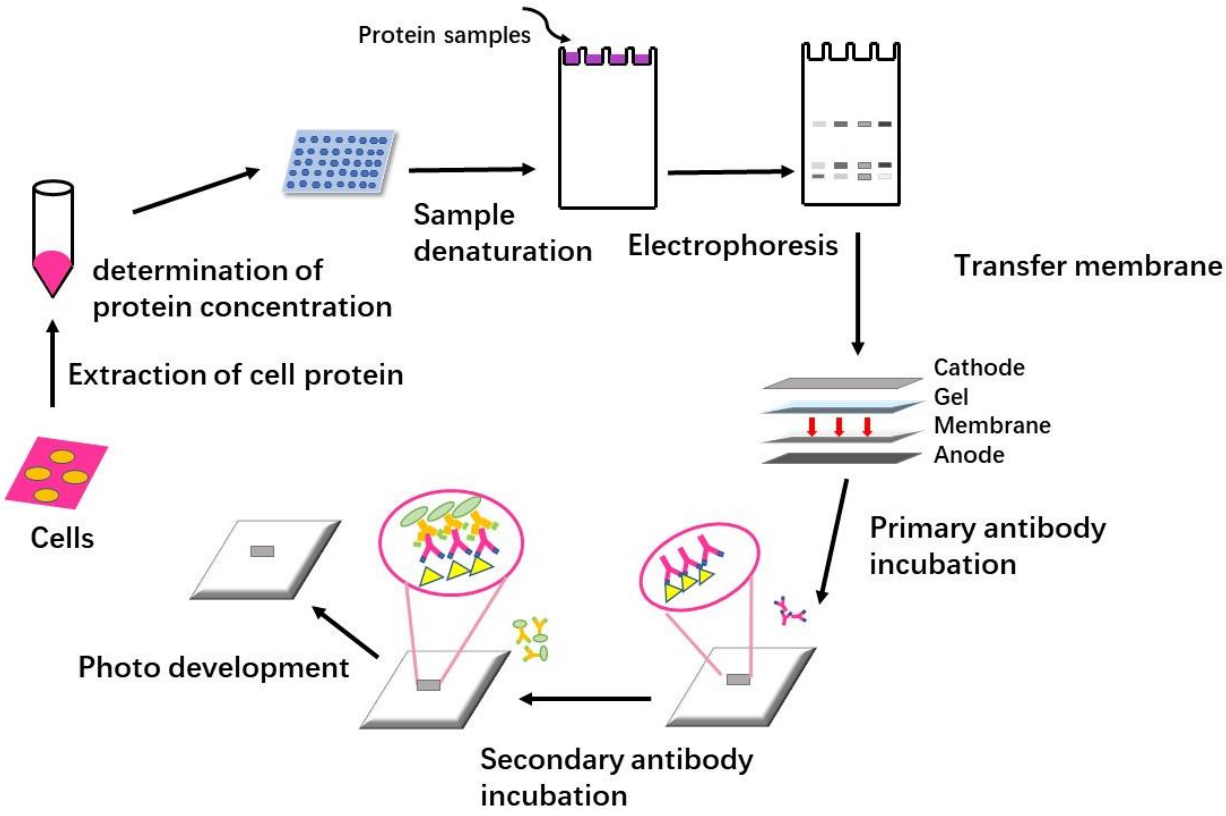

Figure 11: Basic operation process of LC3B protein expression by Western Blot.

2.2.9 Senescence staining

In 1995, Gp Dimri et al. first proposed the senescence related β-hemiactosidase (senescence-as-sociated β-galactosidase, SA-β-gal), which has been widely used as an effective indicator to identify senescent cells. At a pH value of 6.0, SA-β-gal can specifically recognize senescent cells, and the positive rate of staining increased with the increase of senescence(Kurz et al., 2000).

Specific operation steps are as follows:

(1) Adherent cells cultured in 6-well plates, original cell culture medium was removed. BMSCs monolayers washed with PBS for 3 times. Then 1 mL 4% PFA was added, and fixed for 15 min at room temperature.

(2) The cell fixation solution was removed and washed with 2 mL PBS for 3 times, each time for 3 min.

(3) PBS was removed, and 1 mL of the dyeing liquid was added to each hole of the six- well plate.

(4) The six-well plate was placed in the incubator at 37 ℃ overnight and sealed with parafilm sealing membrane to prevent evaporation. Overnight incubation is not allowed in a carbon dioxide incubator. If the color is not obvious, the incubation time can be extended appropriately, but should not exceed 48 h, otherwise false positive results will occur.

(5) Photographs were taken under Keyence microscope. If it is not possible to observe and take photos in time, 2 mL PBS can be added after the dye working fluid is removed and stored at 4 ℃ for several days. Nuclei were stained by Hoechst for quantification.

2.2.10 Statistical Analysis

All data were analyzed with GraphPad Prism 7 and the p-values were calculated with t-test, one-way ANOVA, with significance at values of $p < 0.05$.

3 Results

3.1 Induction of lipid droplets in L87 cells after low or high dose X-irradiation

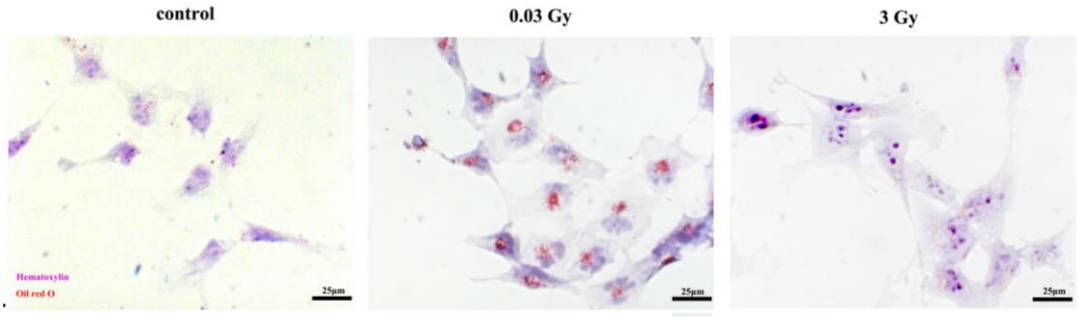

Figure 12: Representative images of L87 exposure to different doses of radiation. Oil red O staining; Lipid droplets were stained with Oil red O. Hematoxylin stained blue nuclei. Nuclei were strained blue with hematoxylin. Scale bar: 25 μm.

I used different doses (0.03 Gy, 3 Gy) to investigate the relationship among radiation, autophagy and lipid droplets. After comparison of multiple doses, we concluded that lipid droplets disappeared under 3 Gy radiation (Figure 12). Therefore, we determined that the radiation dose of 3 Gy was the optimal dose to induce autophagy. Thus, the radiation dosage of 3 Gy was chosen for this study to induce autophagy.

When I kept the cells after low-dose X-irradiation for 2 hours at NO-FBS concentration, LDs went back to background level (Figure 13), suggesting that 30mGy is not sufficient to trigger autophagy.

3.2 Induction of lipid droplets in L87 cells after repeated, multiple low dose X-irradiation

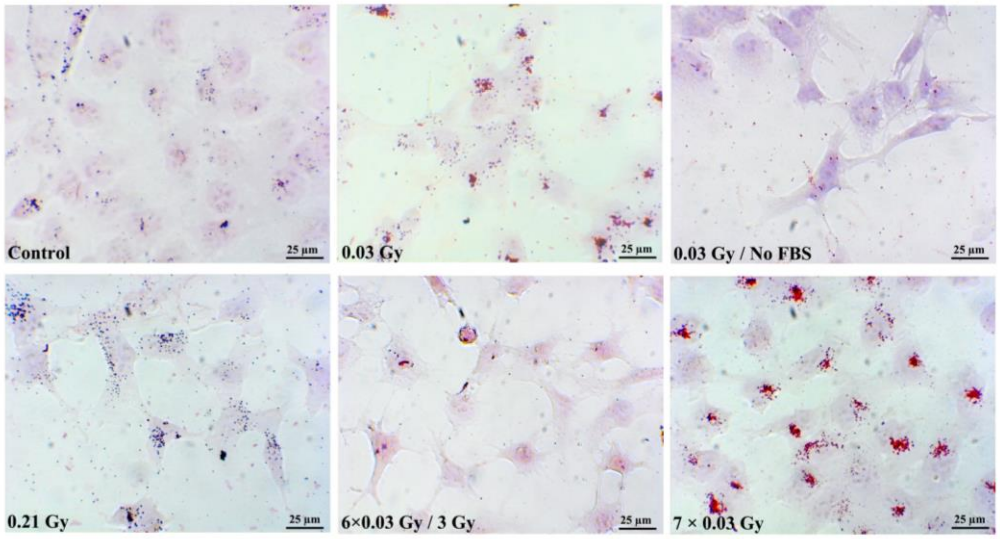

Figure 13: Visualization of lipid droplets (oil red O) in L87 cells. L87 cells were exposed to different doses irradiation. 18 h after treatment the cell were fixed and stained with Oil Red O (red), counterstained with hematoxylin (purple). Images are representatives of three independent experiments. Scale bar: 25 µm.

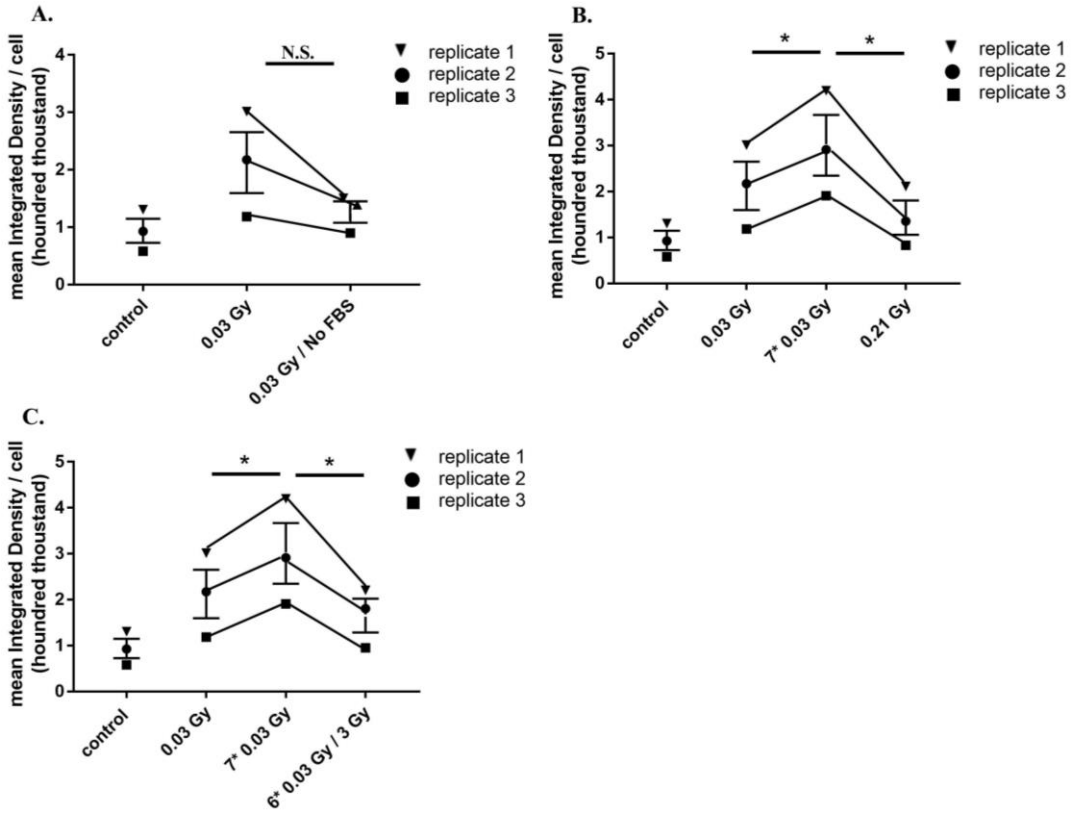

Figure 14: Effects of different doses radiation in lipid droplet of L87. 100 cells were counted and images obtained from three independent experiments. Lipid droplets were quantified with Image J by measuring the integrated density. Data is shown as mean ± SEM (*, $p < 0.05$; N.S., no significant difference) (t-test).

In order to investigate the effect of low radiation doses more closely, an experiment was carried out in which the cells were repeatedly exposed to multiple fractions of a low X-ray dose, with 8 or 16 hours incubation steps in between. The entire irradiation experiment therefore took four days.

Representative images of the Oil red O staining are presented in Figure 13. The according quantification was done by ImageJ and is displayed in Figure 14.

Cells treated with 0.03 Gy have more lipid droplets than the control cells (Figure14 A). Multiple low dose X-irradiation (7×0.03 Gy) generated significantly more lipid droplets as compared with the same total dose (0.21 Gy)(*, $p < 0.05$) (Figure 14 B). After adding a high dose of 3 Gy to previous multiple low dose treatment, cleared lipid droplets (*, $p < 0.05$) (Figure 14 C). This suggests that repeated exposures to low dose irradiation will lead to accumulation of oxidative stress and lipid droplets, without initiating cellular clearing mechanism.

3.3 Identification of radiation-induced autophagy by LC3B immunofluorescence in L87 cells.

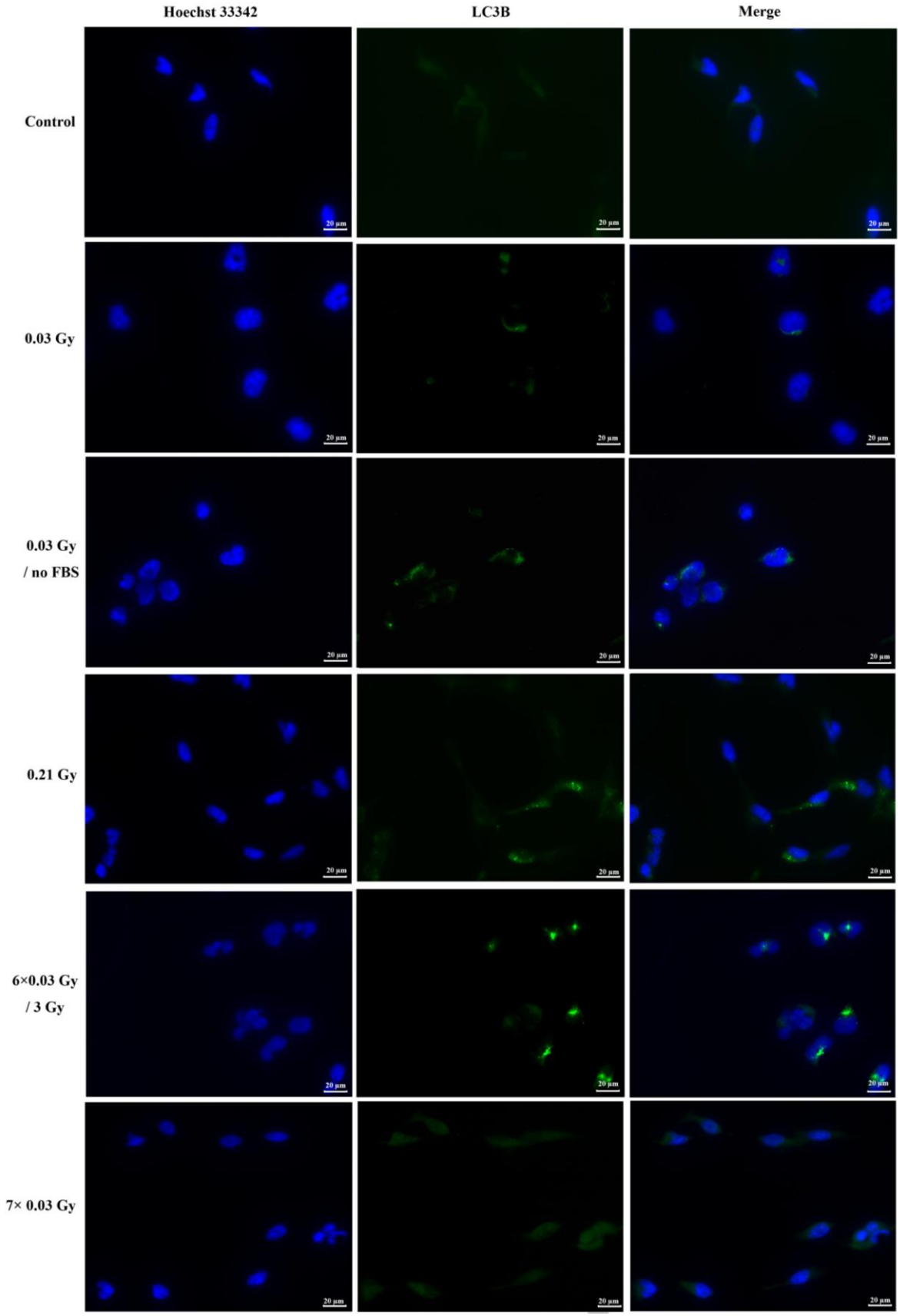

Figure 15: Visualization of autophagy (immunofluorescence LC3B) in L87 cells. L87 cells were exposed to different doses irradiation. For detecting autophagy cells were fixed 18h after treatment and anti-LC3B antibody was used for immunofluorescence. Scale bar: 20 µm.

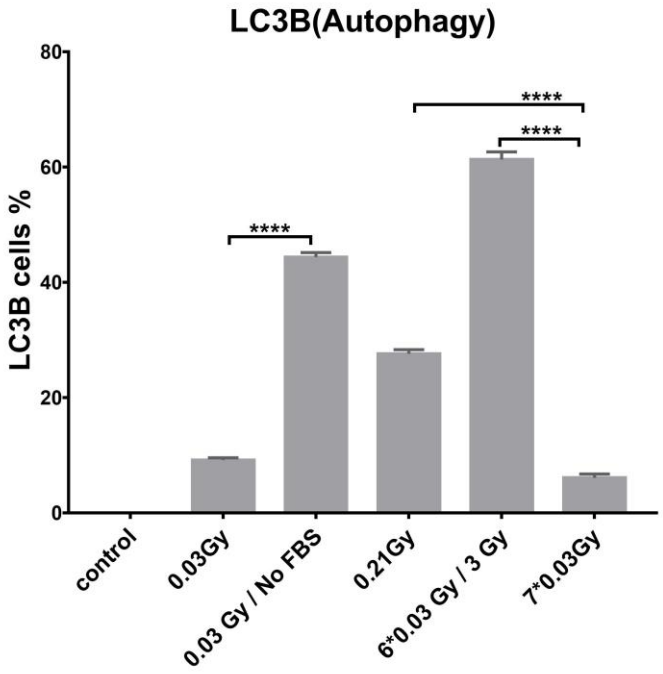

Figure 16: Effects of different doses radiation in autophagy of L87. Images obtained from three independent experiments. LC3B positive cells were evaluated by fluorescence microscopy and positive cells were counted. Data is shown as mean ± SEM (****, $p < 0.0001$) (one-way ANOVA)

To monitor the process of autophagy LC3B was used for immunofluorescence. Medium without FBS was used as a starvation condition to induce autophagy in irradiated cells. Representative images of the immunofluorescence LC3B staining are presented in Figure 15. The according quantification was done by ImageJ and is displayed in the Figure 16.

It could be observed that autophagy is induced significantly by starvation (0.03 Gy / No FBS) compared to 0.03 Gy. As it is also visible in Figure 16 almost 50% show a green fluorescence signal. After 0.21 Gy irradiation, autophagy is significantly increased compared to 7 × 0.03 Gy. Furthermore, it could be shown that only high

doses(6×0.03 Gy / 3 Gy) are able to induce autophagy, whereas low doses impair the autophagy process.

To sum it up, autophagy induced by starvation and high dose irradiation prevents the cell from damage caused by an oxidative stress environment. Multiple low doses irradiation cannot switch on autophagy.

3.4 Staining for carbonylation in irradiated L87 cells

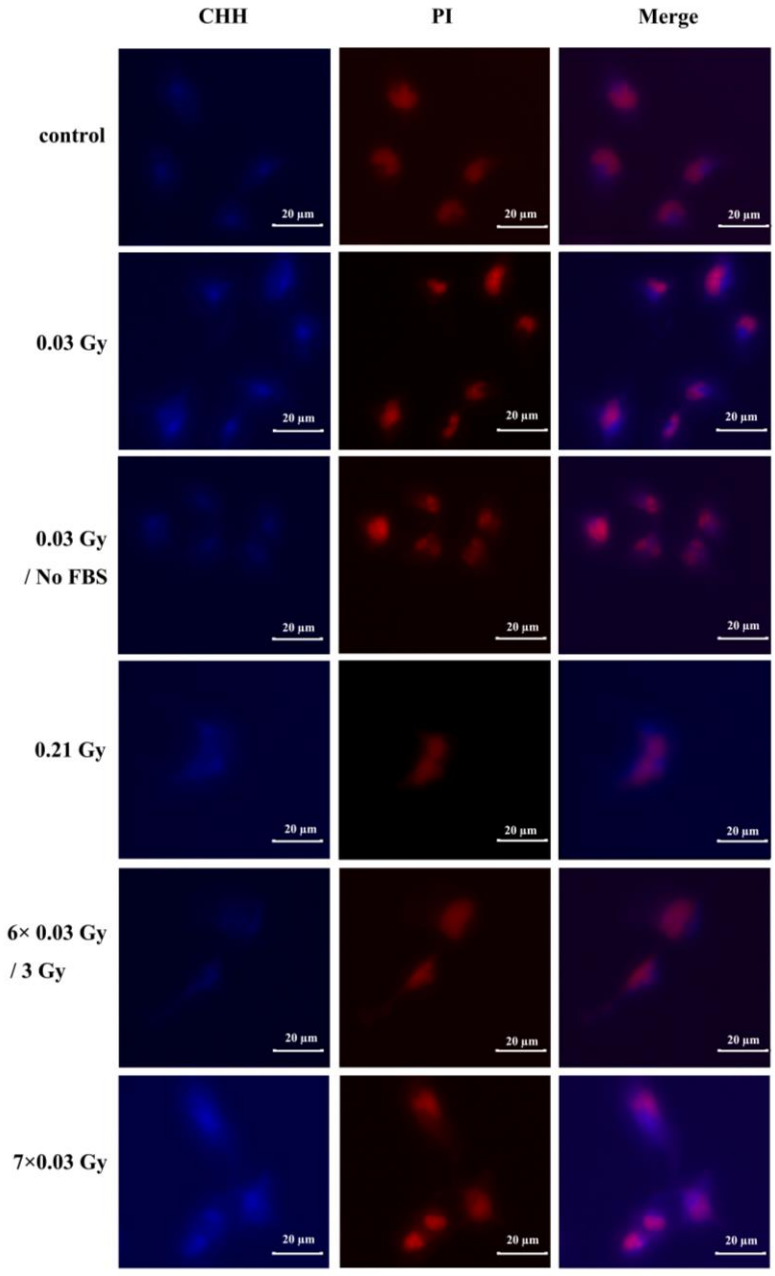

Figure 17: Fluorescence staining of CHH labeling of L87. Fluorescence intensity of CHH (blue) and PI (red). Scale bar: 20 µm.

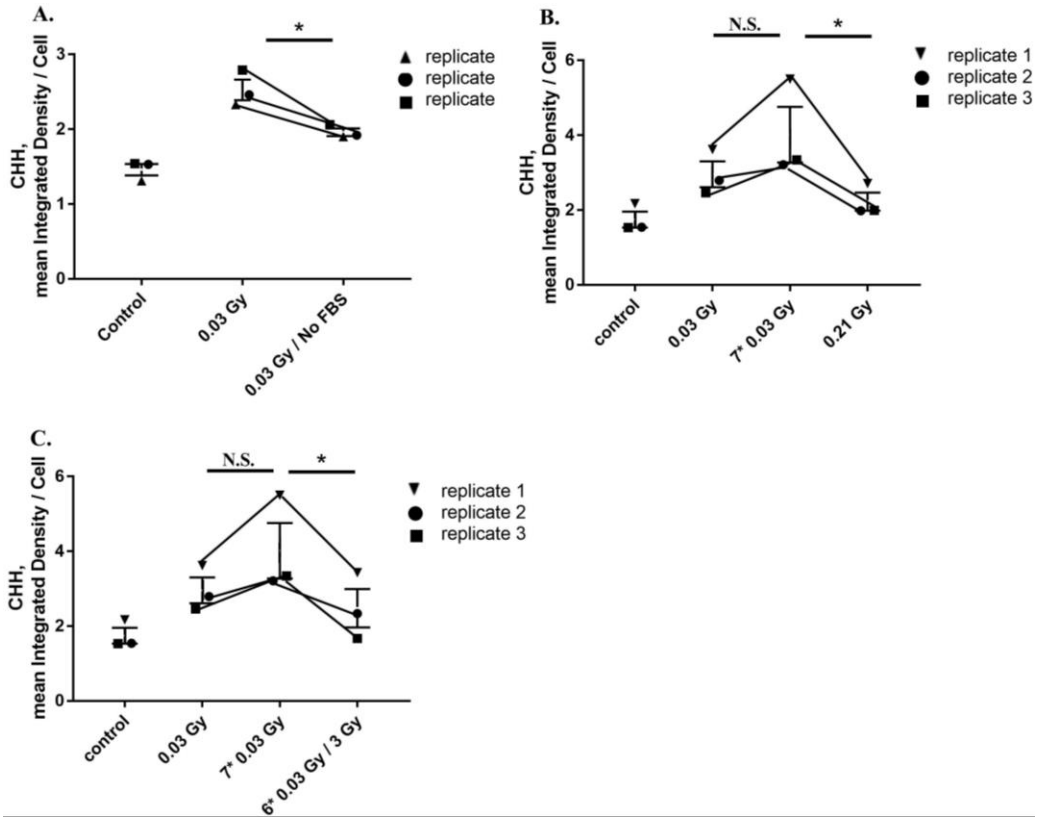

Figure 18: Effects of different doses radiation in carbonylation of L87. 100 cells were counted and images obtained from three independent experiments. Carbonylation levels were given in corrected total cell fluorescence, CTCF =Integrated Density- (Cell Area × Mean Background Fluorescence). Data is shown as mean ±SEM (*, $p < 0.05$; N.S., no significant difference) (t-test)

Intracellular carbonylation reaction includes carbonyl modification of proteins, lipids, and carbohydrates under oxidative stress, which is the most commonly used biomarker of oxidative damage(Dalle-Donne et al., 2003; Dalle-Donne et al., 2006; Zheng et al., 2010). To assess oxidative stress in cells after radiation treatment, the carbonylation of biomolecules was monitored using a fluorescent probe 7-(diethylamino) - coumarin -3- carbonyl hydrazide (CHH). In Representative images of the fluorescence staining of CHH labeling are presented in Figure 17. The according quantification was done by ImageJ and is displayed in the Figure 18.

The carbonylation level of 0.03 Gy / No FBS is significant reduction compared to 0.03 Gy treated cell(*, $p < 0.05$) (Figure 18A). CHH intensity was reached after multi-low doses radiation(7×0.03 Gy) and resulted in more oxidative damage than a higher single dose of 0.21 Gy (*, $p < 0.05$) (Figure 18B). Furthermore, adding a high dose of 3 Gy to six-time radiation of 0.03 Gy result reduction of carbonylation levels significantly compared to seven-time low dose irradiation (*, $p < 0.05$) (Figure 18C).

The result of the CHH labeling experiment indicates that low dose irradiation (0.03 Gy) increases ROS and an environment based on oxidative stress is established.

3.5 mRNA expression of adipocyte transcriptional factors of L87 cells compared with hAMSCs

In a study on murine MSCs after low-dose γ-irradiation an increase of spontaneous (non-induced) adipogenesis was found (Rosemann M et al 2016).

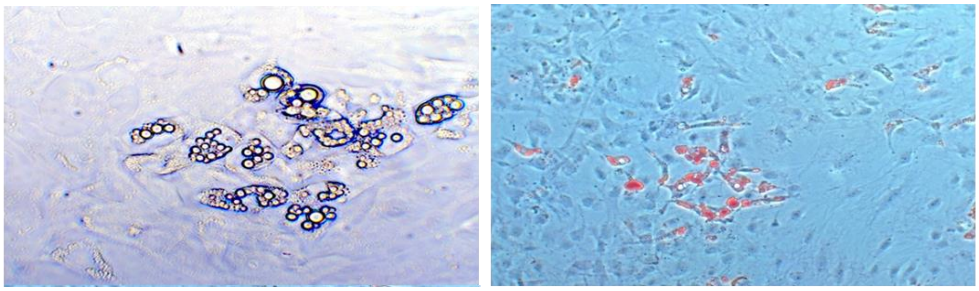

Figure 19: Premature adipogenic differentiation of murine MSCs after low-dose γ-irradiation.

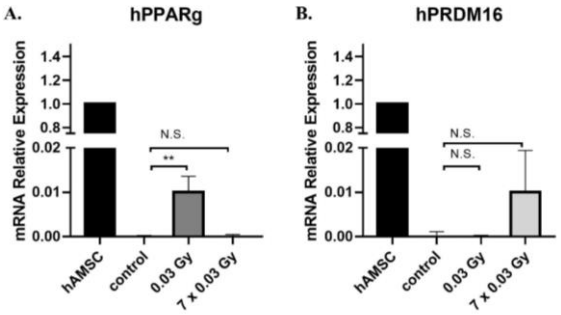

Figure 20: Expression of different adipocyte transcriptional factors in L87 cells relative to the expression in hAMSCs. mRNA relative expression of L87 cells after

different treatments compared to hAMSCs. L87 cells were irradiated at 0.03 Gy, seven times 0.03 Gy or control. After 18 hours the cells were followed by RNA extraction. **A.** mRNA relative expression of hPPARg. **B.** mRNA relative expression of hPRDM16. The data presented are from three replicates as mean ± SEM. N.S., no significant difference (**, $p < 0.01$) (one-way ANOVA).

We therefore wanted to test whether the increase of LDs in low-dose X-irradiated human MSCs could also be associated with the differentiation towards adipocytes. For this, I measured the expression of adipogenesis-specific transcription factors PPARg and PRDM16, and compared them with the expression of these genes in preadipocytes of human adipose derived stem cells.

To investigate whether lipid droplets in irradiated L87 cells were preadipocytes, different adipogenic transcriptional factors were measured. Housekeeping gene GAPDH was used as an internal control. The primers used to detect the indicated gene are hPPARg and hPRDM16.

In order to exclude the formation of lipid droplets due to differentiation of mesenchymal stem cells into adipocytes, the gene expression was investigated using qPCR. Two adipogenic transcription factors were measured for this purpose. hPPARg (Figure 20A) is one important transcription factor for differentiation into adipocytes. The result indicates that L87 cells after single and multiple low dose radiation, where lipid droplets are dominant, do not express hPPARg compared to preadipocytes of hAMSCs.

The same observation can be made for hPRDM16 (Figure 20B). PRDM16 is important for transcriptional regulation of brown and beige adipocyte development(Kajimura, 2015). There is no expression of hPRDM16 in L87 compared to preadipocytes hAMSCs. Therefore, no expression of this gene in L87 supports the statement that there is no differentiation of L87 into an adipogenic direction.

3.6 Identification of LC3B signal in primary human BM-MSCs

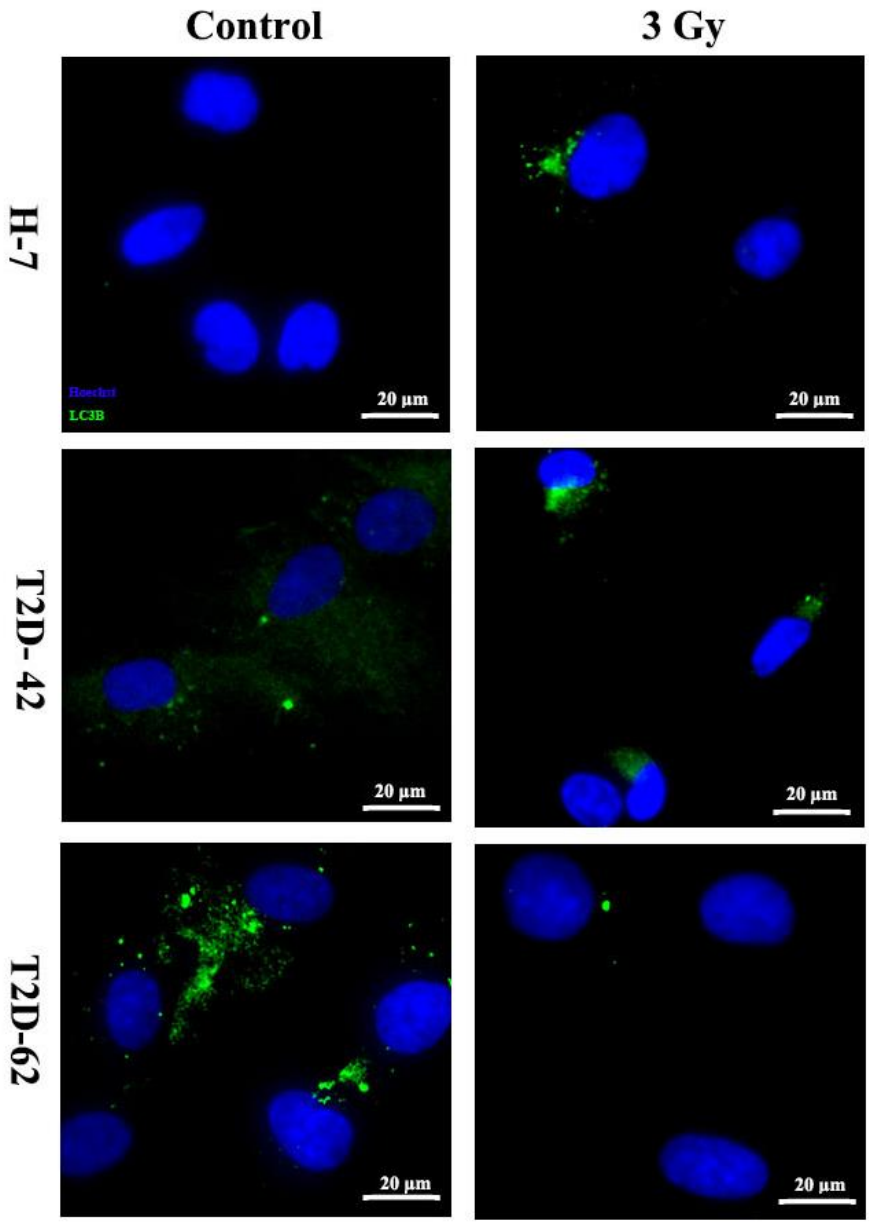

Figure 21: Representative merged images of LC3B in Human MSCs after exposure to 3 Gy radiation. Blue spots indicated Hoechst 33342 DNA staining, and green spots indicated LC3B staining. H-7 represented healthy donors, and T2D-42, and T2D-62 represented type 2 diabetes donors. Cells with green spots represented autophagsomes. Spots of LC3B in cells were observed by fluorescence microscope. Human MSCs were collected 24 h after radiation. Scale bar: 20 µm.

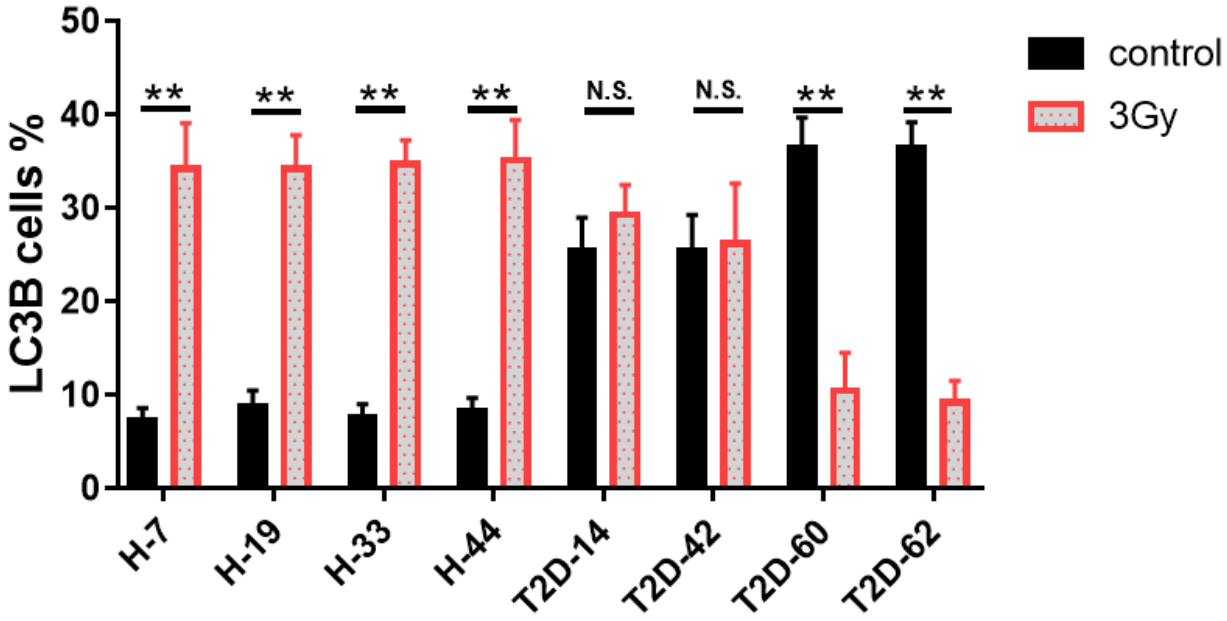

Figure 22: The percent of cells with LC3B spots in Human MSCs after exposure to 3 Gy radiation. H-7, H-19, H-33 and H-44 represented healthy donors; T2D-14, T2D-42, T2D-60 and T2D-62 represented type 2 diabetes donors. Error bars represent mean ± SD. *p< 0.05, **p< 0.01, N.S., no significant difference (t-test).

Healthy Donor								
Number	**H-7**		**H-19**		**H-33**		**H-44**	
Group	**Control**	**3 Gy**	**Control**	**3 Gy**	**Control**	**3 Gy**	**Control**	**3 Gy**
Mean ± SD（%）	**7.2±1.4**	**34.2±4.9**	**8.7±1.7**	**34.2±3.6**	**7.6±1.4**	**34.7±2.5**	**8.2±1.5**	**35.1±4.3**
Difference（%）	**27.0**		**25.5**		**27.1**		**26.9**	
Type 2 diabetes Donor								
Number	**T2D-14**		**T2D-42**		**T2D-60**		**T2D-62**	
Group	**Control**	**3 Gy**	**Control**	**3 Gy**	**Control**	**3 Gy**	**Control**	**3 Gy**
Mean ± SD（%）	**25.5±3.7**	**29.2±3.2**	**25.4±3.8**	**26.2±6.4**	**36.4±3.3**	**10.4±4.1**	**36.5±2.7**	**9.1±2.3**
Difference（%）	**3.7**		**0.8**		**-25.9**		**-27.3**	

Table 5: The LC3B cells percentage change in Human BMSCs after exposure to 3 Gy radiation. H-7, H-19, H-33 and H-44 represented healthy donors; T2D-14, T2D-42, T2D-60 and T2D-62 represented type 2 diabetes donors.

Several studies have shown that radiation is a stable condition for inducing autophagy [21]. We used immuno- and western blotting to evaluate autophagy in Human BMSCs. After preliminary experiments, we determined that the radiation dose of 3 Gy can stably induce autophagy of BMSCs. To test autophagy in BMSCs, we first examined spots distribution of LC3B under fluorescence microscope. LC3B activity was positively correlated with autophagy level. It was a recognized marker of reflected autophagy activity. Representative merged images of LC3B in Human MSCs after exposure to 3 Gy radiation are presented in Figure 21.

After radiation, LC3B cells percentage increased significantly in healthy donors-3 Gy groups, compared with healthy donors control group ($p < 0.05$) (Figure 22), which resulted in differences ranging from 25.5% to 27.1%.

In T2D donors control group, LC3B cells percentages were significantly higher than healthy donors control group. After radiation, LC3B cells percentages of T2D donors 3 Gy groups had no significant difference from T2D donors control group.

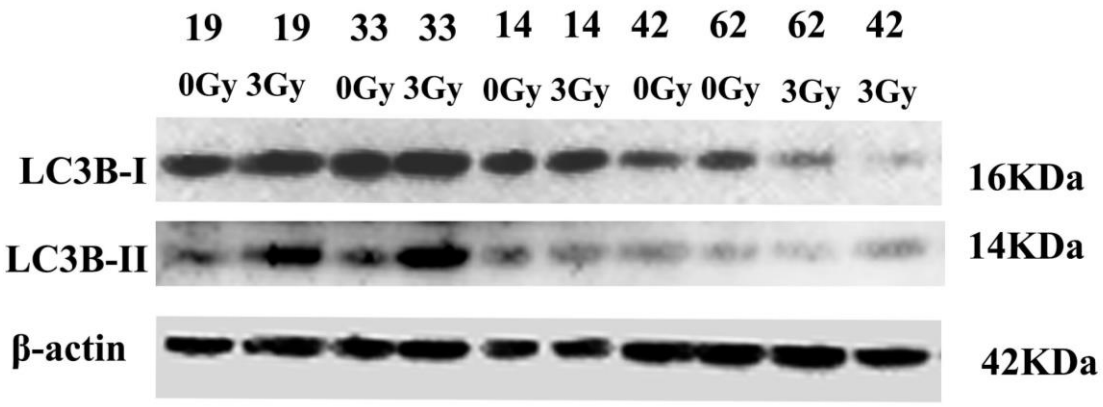

Figure 23: Radiation-induced autophagy in Human-BMSCs. Human-BMSCs were treated with 3 Gy radiation. The western blotting analysis was used to detect the expression of autophagy relative proteins, including LC3B-I, LC3B-II. The β-actin

served as a loading control. 19 and 33 represented healthy donors, and 14, 42, and 62 represented type 2 diabetes donors.

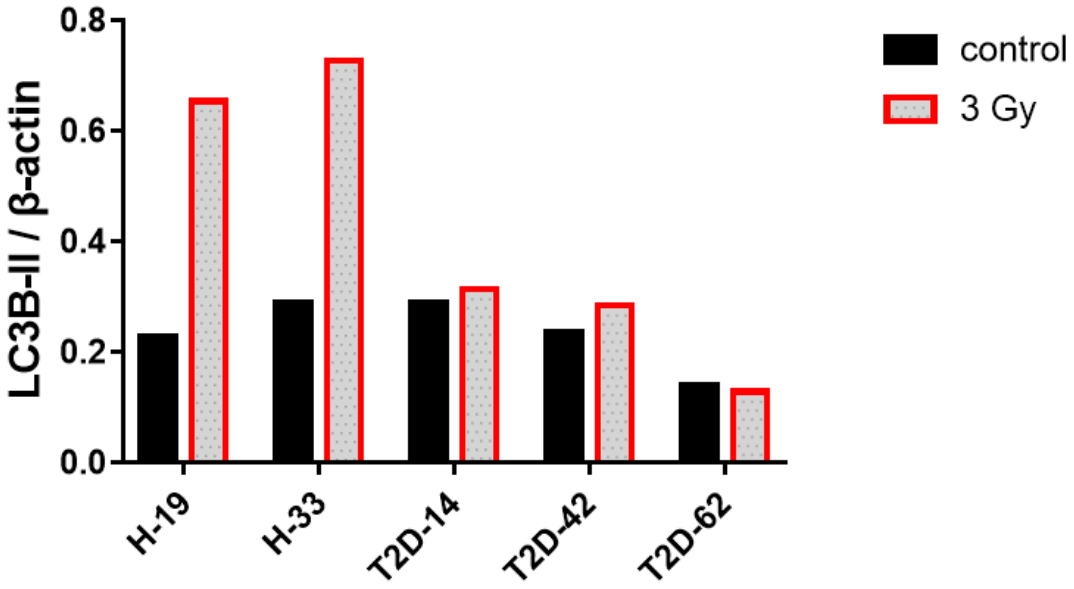

Figure 24: LC3B-Ⅱ/ β-actin protein content ratio gray-analysis. The β-actin served as a loading control. H-19 and H-33 represented healthy donors, and T2D-14, T2D-42, and T2D-62 represented type 2 diabetes donors.

Another method of monitoring LC3B autophagy was through western blotting. Analysis of two bands: LC3B-I (16 kD) and LC3B-II (14 kD). LC3B-I proteins are mainly distributed in cell cytoplasm. When autophagosome was formed, LC3B-I and phosphatidyl ethanolamine (PE) facilitated LC3B-II coupling. It has the ability of membrane localization and the localization of autophagosome in inner membrane and outer membrane. Once autophagy body was fused with lysosomes, LC3B-II in autophagosome was degraded by hydrolases in lysosomes. Therefore, the level of LC3B-II or LC3B-II/LC3B-I ratio change reflects the changes of autophagy activity [14]. The level of LC3B-II also reflects the number of autophagosomes. Increased LC3B-II levels may be due to induction or blocked autophagy(Tanida et al., 2005).

In our results, radiation induced increase of LC3B-II levels in Human donors 3 Gy group. LC3B-II levels were suppressed in T2D donors 3 Gy group after radiation, compared with T2D donors control group (Figure 23, Figure 24).

In summary, all these data suggested that radiation could induce autophagy in healthy donor BMSCs, which was suppressed in T2D patients.

3.7 Quantification of oil red cells in Human BMSCs after 3 Gy radiation.

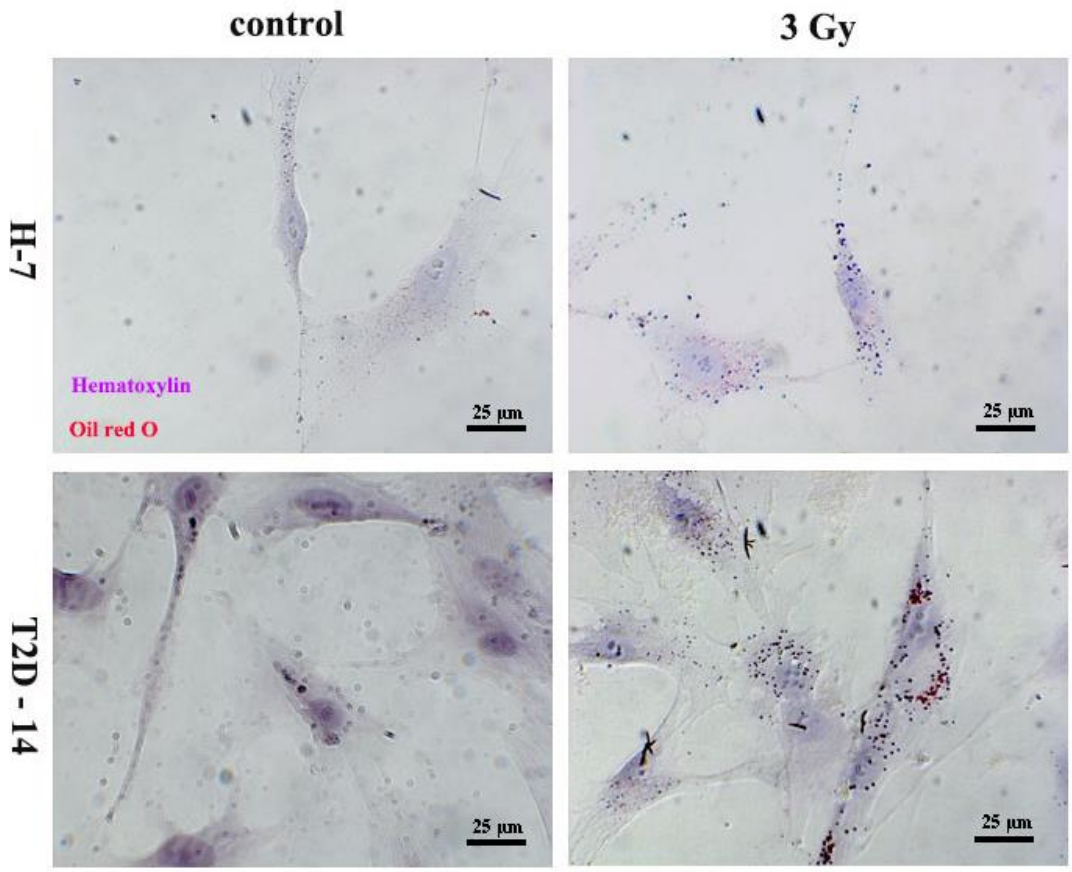

Figure 25: Representative images of Oil red O staining in Human MSCs after 3 Gy radiation. Lipid droplets stained with Oil red O staining were clearly visible in human-BMSCs, showing various lipid droplet sizes. Hematoxylin was stained blue nuclei. H-7 represented a healthy donor, and T2D-14 represented type 2 diabetes donors. Human MSCs were collected at 24 h after radiation. Scale bar: 25 µm.

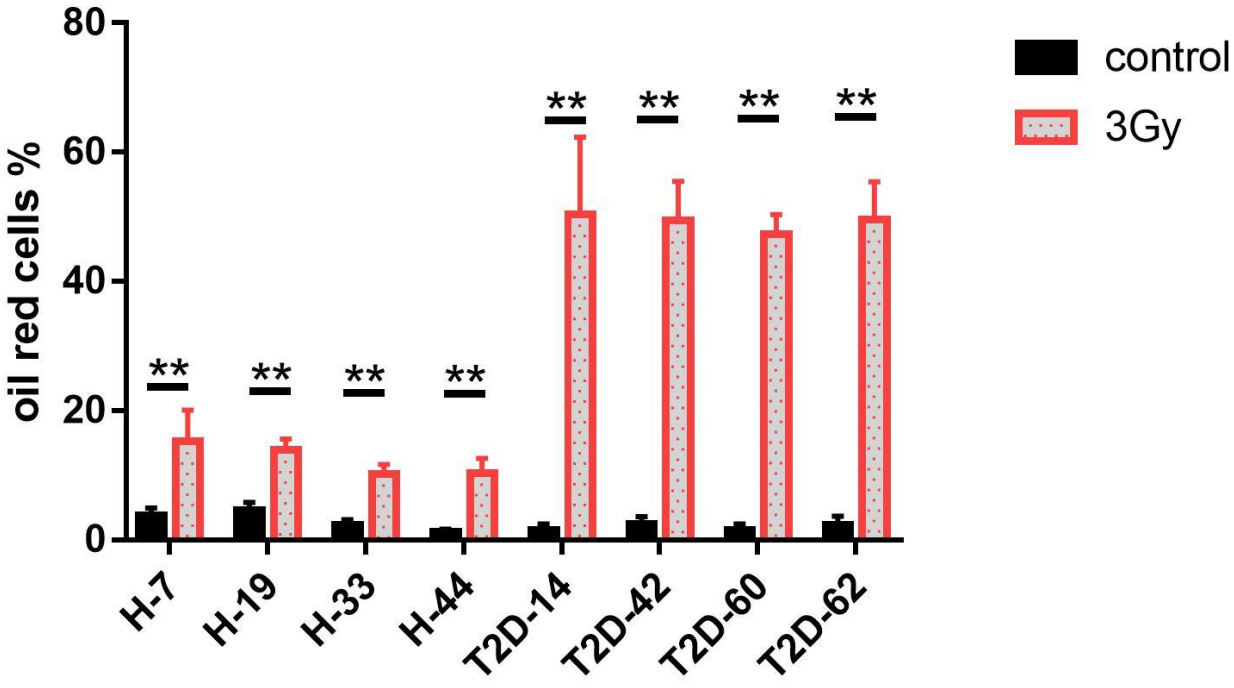

Figure 26: Quantification of oil red cells in Human BMSCs after 3 Gy radiation. H-7, H-19, H-33 and H-44 represented healthy donors, and T2D-14, T2D-42, T2D-60 and T2D-62 represented type 2 diabetes donors. Error bars represented mean ±SD. *p< 0.05, **p< 0.01 (t-test).

Healthy Donor								
Number	**H-7**		**H-19**		**H-33**		**H-44**	
Group	**Control**	**3 Gy**	**Control**	**3 Gy**	**Control**	**3 Gy**	**Control**	**3 Gy**
Mean ± SD（%）	**3.8±1.1**	**15.3±4.8**	**4.6±1.2**	**13.9±1.7**	**2.3±0.8**	**10.2±1.4**	**1.3±0.4**	**10.4±2.3**
Difference（%）	**11.4**		**9.3**		**7.9**		**9.1**	
Type 2 diabetes Donor								
Number	**T2D-14**		**T2D-42**		**T2D-60**		**T2D-62**	
Group	**Control**	**3 Gy**	**Control**	**3 Gy**	**Control**	**3 Gy**	**Control**	**3 Gy**
Mean ± SD（%）	**1.5±0.9**	**50.4±11.9**	**2.5±1.1**	**49.4±6.1**	**1.5±1**	**47.3±3.1**	**2.3±1.4**	**49.6±5.8**
Difference（%）	**48.9**		**46.9**		**45.8**		**47.3**	

Table 6: The oil red o cells percentage changes in Human BMSCs after 3 Gy radiation. H-7, H-19, H-33 and H-44 represented healthy donors, and T2D-14, T2D-42, T2D-60 and T2D-62 represented type 2 diabetes donors.

Oil red O is highly soluble in fat and can specifically stain neutral fat such as triglyceride in tissue. Hematoxylin staining provides histological information, while Oil red O staining shows the size and location of lipid droplets in cells. Representative images of Oil red O staining in Human MSCs after 3 Gy radiation are presented in Figure 25.

In T2D donors control group, oil red cells percentages were almost the same as those of healthy donors control group. After radiation, oil red cells percentages all increased in Healthy and T2D 3Gy cells, compared with the control group. Healthy donors 3 Gy cells increased significantly by a range of 7.9% to 11.4%, compared with control group ($p < 0.01$). T2D donors 3 Gy cells increased significantly by a range of 45.8% to 48.9%, compared with control group ($p < 0.01$). T2D-BMSCs 3Gy cells were stained much more intensively than Healthy-BMSCs 3Gy cells (Figure 25).

3.8 Senescence in different donors

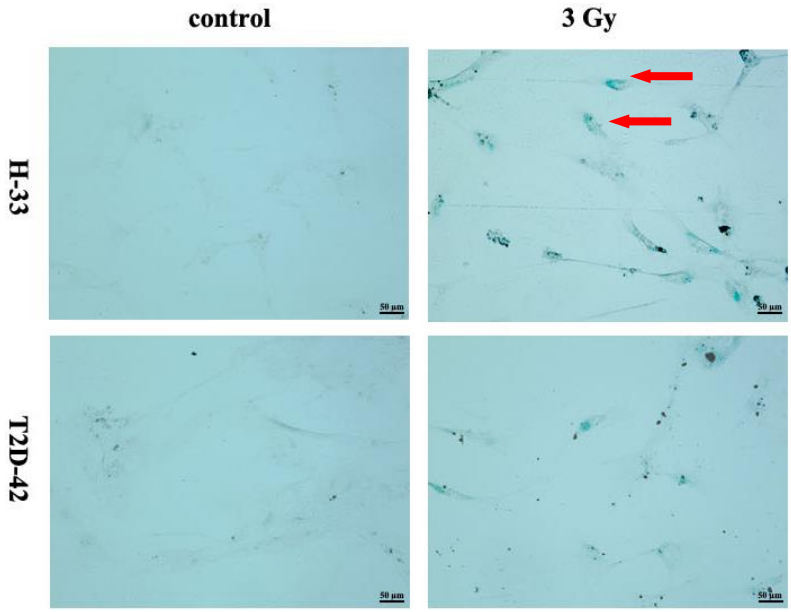

Figure 27: Senescence in Human-BMSCs after 3 Gy radiation. Representative images of Human-BMSCs after SA-β-gal staining to detect senescence induction. Blue spots indicated senescent cells. H-33 represented a healthy donor, and T2D-42 represented a type 2 diabetes donor. Human-BMSCs were collected at 7 days after radiation. Scale bar: 50µm

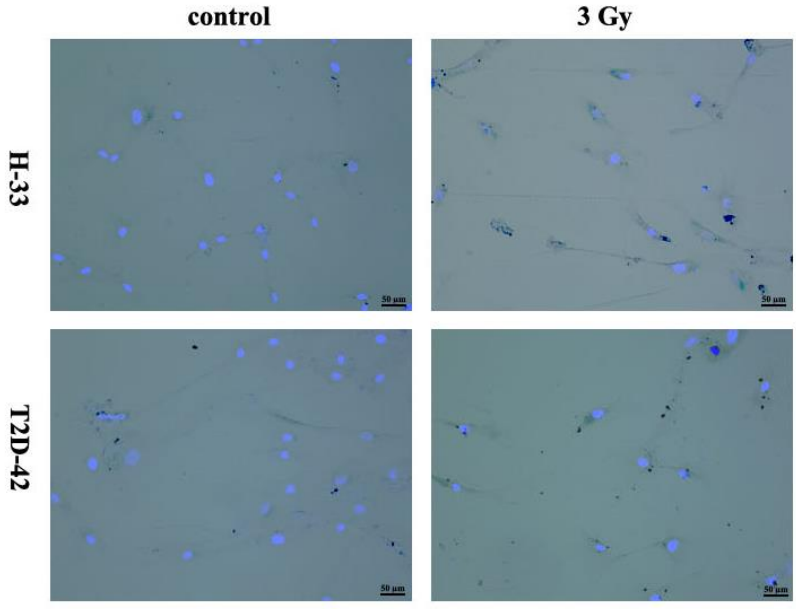

Figure 28: Counterstaining nuclei for quantify senescence cells percentage in Human-BMSCs. Representative images of Human-BMSCs after SA-β-gal-staining to detect senescence induction. H-33 represented a healthy donor, and T2D-42

represented a type 2 diabetes donor. Human-BMSCs were collected at 7 days after radiation. Nuclei were counterstained with Hoechst33342. Scale bar: 50 μm

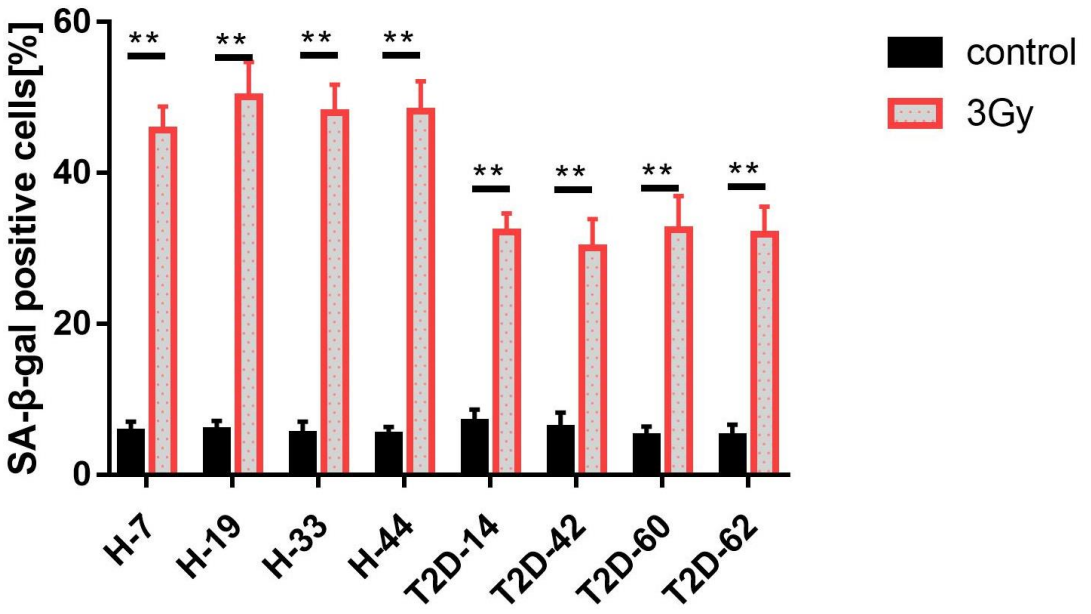

Figure 29: Quantification of senescence cells in Human BMSCs after 3 Gy radiation. H-7, H-19, H-33 and H-44 represented healthy donors, and T2D-14, T2D-42, T2D-60 and T2D-62 represented type 2 diabetes donors. Error bars represent mean ± SD. *p< 0.05, **p< 0.01 (t-test).

Healthy Donor								
Number	**H-7**		**H-19**		**H-33**		**H-44**	
Group	**Control**	**3 Gy**	**Control**	**3 Gy**	**Control**	**3 Gy**	**Control**	**3 Gy**
Mean ± SD（%）	**5.7±1.4**	**45.7± 3.1**	**5.9±1.3**	**50.1± 4.6**	**5.4±1.6**	**48.0± 3.7**	**5.3±1.1**	**48.2± 3.9**
Difference（%）	**40.1**		**44.0**		**42.0**		**43.0**	
Type 2 diabetes Donor								
Number	**T2D-14**		**T2D-42**		**T2D-60**		**T2D-62**	
Group	**Control**	**3 Gy**	**Control**	**3 Gy**	**Control**	**3 Gy**	**Control**	**3 Gy**
Mean ± SD（%）	**7.0±1.7**	**32.2± 2.4**	**6.2±2.0**	**30.1± 3.8**	**5.1±1.3**	**32.5± 4.4**	**5.1±1.6**	**31.9± 3.7**
Difference（%）	**25.2**		**23.9**		**27.4**		**26.8**	

Table 7: Senescence cells percentage changes in Human BMSCs after 3 Gy radiation. H-7, H-19, H-33 and H-44 represented healthy donors, and T2D-14, T2D-42, T2D-60 and T2D-62 represented type 2 diabetes donors.

As the basic unit of biological senescence, cell senescence plays an increasingly important role in anti-senescence research. Because of its simple operation and obvious specificity, SA-β-gal has been widely applied to detect senescent cells in vivo and in vitro. It has been confirmed that SA-β-gal is GLBl product of lysosomal β-gal gene. At the pH value of 4.5, the activity of β-gal was highest, and at the pH value of 6.0, SA-β-gal was tested positive (Kurz et al., 2000).

In this study, the cells were cultured for 1 week after radiation treatment. Representative senescence staining images are shown in the Figure 27, Figure28. A hundred cells were randomly selected from different groups, with no less than 6 randomly selected regions. Human BMSCs were quantified by one people and the percentage of positive senescent cells in total cells was determined.

Human BMSCs cultured for 1 week after radiation showed increase of SA-β-gal- cells in both Healthy and T2D groups. Under the same radiation stress condition, healthy BMSCs had more senescent cells.

3.9 DNA repair foci formation in Human-BMSCs after radiation

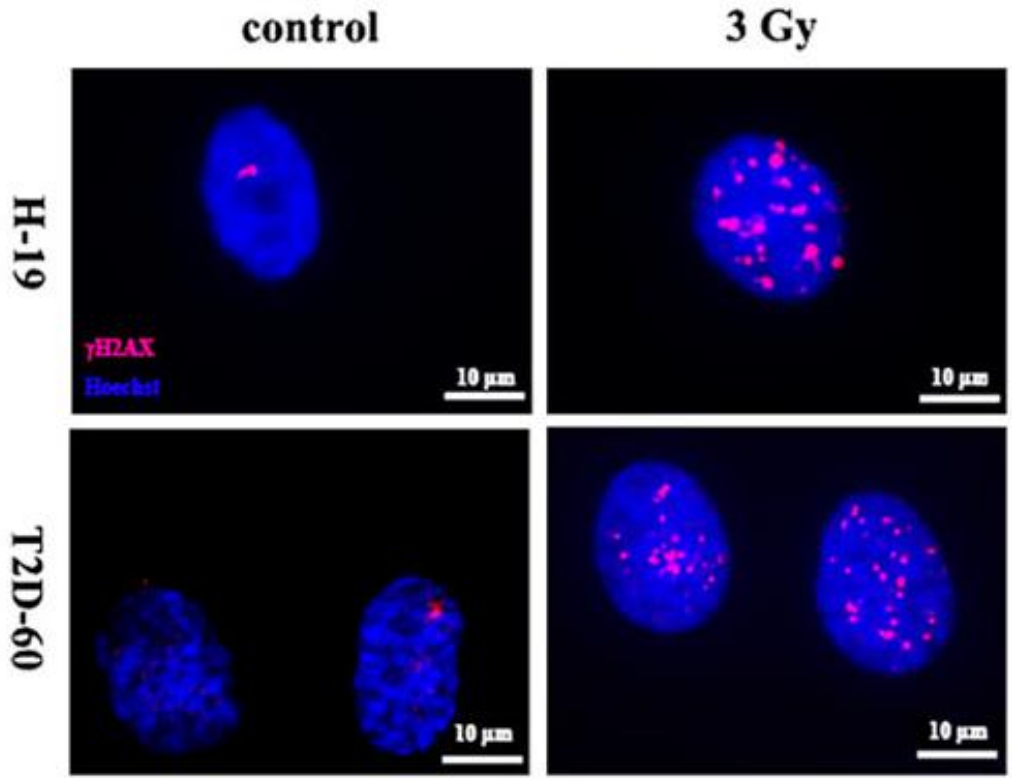

Figure 30: Representative merged images of γH2AX foci formation in Human BMSCs after exposure to 3 Gy radiation. Repair foci formation was detected in immunoflourescent stainings of repair proteins γH2AX at 90 minutes after radiation. H-19 represented a healthy donor, and T2D-60 represented a type 2 diabetes donor. Blue spots indicated Hoechst33342 DNA staining, and red spots indicated γH2AX. Scale bar: 10 μm.

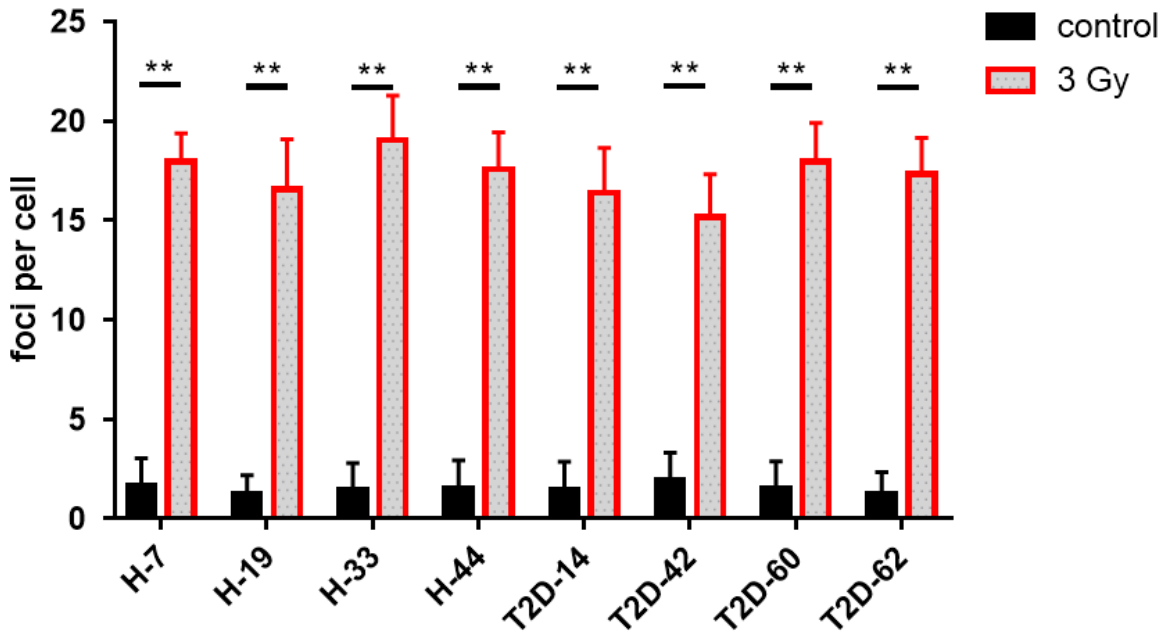

Figure 31: Quantification of γH2AX foci in Human BMSCs after exposure to 3 Gy radiation. H-7, H-19, H-33 and H-44 represented healthy donors, and T2D-14, T2D-42, T2D-60 and T2D-62 represented type 2 diabetes donors. Error bars represent mean± SD. *p< 0.05, **p< 0.01 (t-test).

Healthy Donor								
Number	**H-7**		**H-19**		**H-33**		**H-44**	
Group	**Control**	**3 Gy**	**Control**	**3 Gy**	**Control**	**3 Gy**	**Control**	**3 Gy**
Mean ± SD（%）	**1.7±1.4**	**18.0±1.4**	**1.2±1.0**	**16.6±2.5**	**1.5±1.3**	**19.0±2.3**	**1.6±1.3**	**17.6±1.9**
Difference（%）	**16.3**		**15.3**		**17.6**		**16.0**	
Type 2 diabetes Donor								
Number	**T2D-14**		**T2D-42**		**T2D-60**		**T2D-62**	
Group	**Control**	**3 Gy**	**Control**	**3 Gy**	**Control**	**3 Gy**	**Control**	**3 Gy**
Mean ± SD（%）	**1.4±1.4**	**16.4±2.3**	**1.9±1.4**	**15.1±2.2**	**1.6±1.4**	**17.9±2.0**	**1.3±1.1**	**17.3±1.8**
Difference（%）	**14.9**		**13.2**		**16.4**		**16.1**	

Table 8: γH2AX foci numbers in Human BMSCs after 3 Gy radiation. H-7, H-19, H-33 and H-44 represented healthy donors, and T2D-14, T2D-42, T2D-60 and T2D-62 represented type 2 diabetes donors.

Ionizing radiation can induce DNA damages and activate the cascade of signals that control DNA repair. DNA damages can lead to single-strand breaks, double stand breaks (DSB) and genetic mutations(Jeggo et al., 2007). The first step of DSB response is the phosphorylation of the histone H2AX which can be quantified via specific γH2AX antibodies by using immunofluorescence. The foci of DSB can be visualized in this way(Paull et al., 2000).

Fluorescence microscopy was used to observe the formation of γH2AX foci in cells after 3 Gy radiation. Random field were selected and at least 100 nuclei were counted for foci quantification. After 90 min, γH2AX foci formation increased in both T2D and healthy radiation groups. The result of 3 Gy radiation treatment did not show any significant difference between foci formations in healthy and T2D BMSCs (Figure 30, Figure 31).

4 DISCUSSION

4.1 Wound healing complications in T2D patients

Wound healing disorders are a common side effect in patients with diabetes mellitus. Up to 10 percent of diabetics develop a chronic wound, in particular a diabetic foot syndrome, in the course of the disease(Orozco-Beltran et al., 2016). In Germany alone, 70 percent of all amputations performed are due to diabetes and the resulting wound healing disorders.

Patients with diabetes are about five times more likely to become infected after surgery than those without diabetes(Shaw et al., 2010). However, not only large, but even the smallest wounds often heal more slowly in diabetics and are prone to inflammation. If such small cutaneous lesions suffer from impaired healing, they frequently turn into chronic wounds, involve larger and larger areas of the dermis and can eventually lead to ulceration (as in diabetic foot syndrome).

One factor involved in the development of chronic wounds in T2D patients are the diabetic vasculopathies as described above. It is generally agreed that the arterial circulatory disorder that affects various tissues in during the development of diabetes is an important contributor to impaired wound healing(Jude et al., 2001). To make matters worse, diabetes damages the nerves. This is why patients often do not feel any vacancies. If these wounds are in places that are difficult to access, e.g. on the sole of the foot, they can remain undetected for some time, become infected and ultimately lead to deep ulcerations. In such cases, professional wound counseling and care is urgently needed to prevent worse things from happening(Vincent et al., 2011).

The reason why wounds heal poorly in people with diabetes could be a slowed down insulin metabolism at the wound site. Until now, vascular and nerve damage and a reduced immune system have been held responsible for the wound healing disorder. A recent study from the Cologne Max Planck Institute for ageing research, however, indicate that a dysregulationn of the insulin/IGF signaling pathway and mTOR/FOXO

could be hold responsible for the wound healing complications, rather than the hyperglycaemia itself(Kakanj et al., 2016).

4.2 Response of MSCs to oxidative stress

As adult stem cells without the possibility to be replaced by more primitive cells, MSCs require sophisticated cellular mechanisms to clean them of toxic metabolic waste products, cellular debris and to repair DNA lesions. One key mechanism to remove macromolecules with irreversible damages is cellular autophagy(Revuelta et al., 2017).

I have shown in my studies that oxidative stress induced by X-irradiation with intermediate doses (210 mGy to 3 Gy) is capable of triggering autophagy in a human MSC cell line (L87). This is characterized by LC3B signals in the cytoplasm.

Interestingly, at a tenfold lower radiation-dose (30mGy), the level of autophagy was also lower, but the MSCs displayed formation of lipid droplets. Cells with these lipid droplets also showed a positive staining with the coumarin CHH, that detects carbonylated lipids and carbonylated proteins. Macromolecules with these carbonyl-adducts are irreversibly damaged and require elimination from the cells. The formation of lipid droplets and carbonylated lipids indicates temporal or permanent defect of the cells to adequately clear of these damaged macromolecules. Accumulation of carbonylated lipids is a potential cause for lipid toxicity.

Interestingly, when several small radiation doses were applied in a fractionated exposure scheme (7 x 30mGy with 8 h or 16 h hours periods between), the level of lipid droplets accumulated more and more.

When these multiple fractions of low doses were followed by a single high dose (3 Gy), autophagy was induced again and the level of lipid droplets decreased. This suggests that either a minimal level of oxidative stress is required in MSCs to switch on autophagy, or that ionizing radiation has to be high enough to induce a DNA damage response in order to trigger autophagy.

It is of relevance to compare this non-linear radiation response of autophagy in MSCs with different exposure scenarios in daily life or in medical practice: This shows that in particular multiple CT-scans (each of which delivers about 15 – 30mSv X-ray dose) have the potential cause accumulation of LDs in MSCs without triggering autophagy (Figure 32).

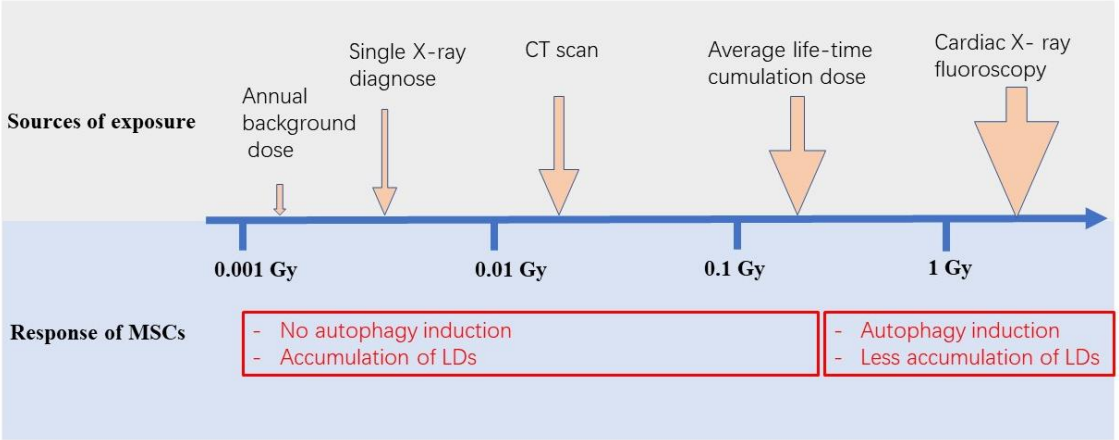

Figure 32: Intracellular response of MSC exposed to different radiation doses.

4.3 Autophagy after ionizing radiation

Autophagy can be activated under adverse environmental conditions such as nutritional deficiencies, reduced growth factors, and hypoxia. Autophagy as a gene-regulated stress response is common in some human cancer cell lines when exposed to ionizing radiation. In contrast to apoptosis, induction of autophagy can be observed in many cell lines after ionizing radiation(S. Shimizu et al., 2014). Unlike apoptosis, autophagy is a pro-survival mechanism and active in many post-mitotic cells such neurons(Suomi et al., 2019), cardiomyocytes(L. Zhou et al., 2016), hepatocytes(Xu et al., 2020), renal epithelial cells(Ding et al., 2015; W. J. Liu et al., 2018) and vascular endothelial cells(Grootaert et al., 2018; K. A. Kim et al., 2018).

Similar to the debate about whether autophagy promotes or inhibits the development of tumors, the autophagy response of cancer cells to radiation shows some different effects in radiotherapy. Radiation therapy induces autophagy in both normal and cancer cells. Studies have reported that in malignant gliomas, breast cancer and

prostate cancer cells, radiotherapy-induced autophagy can cause cell death (Paglin et al., 2001).

Irradiation directly acts on organic molecules causing DNA breakage. Generating free radicals to interact with biological macromolecules to indirectly damage DNA, block cell division and proliferation, and cause irreversible damage. Tumor cells resist these injuries through autophagy, maintain their own stability, and reduce radio sensitivity(Mizushima et al., 2008).

4.4 Autophagy can be induced in L87 cells by X-ray

Only sporadic data are available on the induction of autophagy markers in MSCs after ionizing irradiation. J Hou et al, demonstrated autophagy in umbilical cord derived human MSCs (hUC-MSCs) after irradiation with 6 Gy. The dose of 6 Gy is much higher than anything reasonably used in clinic, and it is a dose that inflicts proliferative cell death in most cells. The hUC-MSCs used in their study are virtually of new born age, and might therefore not necessarily reflect the situation in adult patients(Hou et al., 2013). I therefore determined features of autophagy in MSCs after sub-lethal doses used in medical radiology (30 mGy) and a dose that is used in radio oncology (3 Gy). Also, to have cells studied in my project which are more representative for patients in emergency surgery or plastic surgery, I preferred to use MSCs from donors in the 3rd trimester of life.

Using the L87 cell line (SV40 immortalized MSCs from a 70-year-old male donor) I could show that autophagy induction increases between 0 Gy, 30 mGy and 3 Gy. This is clearly shown both as the number of LC3 positive cells increase, and also by the specify in Western Blot for the LC3b-II protein fragment. Autophagy in MSCs of adult donors was also reported by others, after treating the cells with starvation medium or with rapamycin(Rodriguez-Vargas et al., 2012). In their experiments a decline in the rate of autophagy was observed when MSCs were induced to differentiate. My observation that between an X-ray dose of 30 mGy and 3 Gy the LC3B-II signal in cells increases suggests that autophagy is triggered as part of the

DNA damage response (DDR). This was important for the quantification of induced autophagy in MSCs derived from T2D patients.

4.5 Radiation induced generation of lipid droplets

Despite a small increase of autophagy signal in L87 MSCs after 30mGy, and a much larger level of autophagy induction in these cells after 3Gy X-irradiation, I observed another form of cell response in an almost reciprocal dependency. Between 18 and 24hours after X-irradiation with 30mGy, a dramatic increase in the formation of lipid droplets (LD) was obvious, as detected by staining with neutral fat dye oil-red O. In contrast to oil drops in differentiated adipocytes, radiation induced LDs are higher in number per cell, but much smaller. Since LDs have been described in the literature as appearing after oxidative stress and containing carbonylated neutral fat, I stained them with the carbonyl-specific dye coumarin-hydrazide and indeed found a strong signal indicating carbonylated fatty acids. This suggests that lipid droplets serve as a dedicated structure in MSCs to collect potentially toxic lipids for later processing them in autophagy. Isolation of carbonylated lipids will probably reduce the risk of lipid toxicity at cellular membranes.

Surprisingly, the number and concentration of LDs in MSCs decline after the higher radiation dose of 3 Gy in my experiments. This bi-phasic response of MSCs in terms of LD response suggests that there are two counter-acting mechanisms triggered by radiation, which have a promoting and a protecting effect. It is possible, that the rise in LDs after low doses is a reflection of the increase of ROS, which is known to be low-dose specific, but can saturate at higher doses. This low-dose typical increase of oxidative stress acts on many cellular molecules, such as proteins, membranes and lipids. On the other hand, DNA damage response in cells requires usually higher doses, above 500 mGy. Considering that 1 Gy induces about 20 DNA double-strand breaks, one can estimate that at 30 mGy there are still ~ 50% of cells which stay unaffected at all (assuming Poisson distribution of the DNA breaks in individual cells). This would mean that about 150 mGy is needed to hit 95% of all cells. Therefore,

efficient induction of autophagy might require doses higher than several hundred of mGy, before a linear response can be observed. Therefore, assuming that LD induction follows a promoting mechanism up to a dose of some 10 of mGy, but a protecting mechanism after doses above some hundreds of mGy, a biphasic response with an initial increase to a maximum, followed by a decrease at higher doses would be a natural consequence.

To validate this hypothesis, a subjected the L87 cells to repeated doses of 30 mGy over 4 days (2 fractions per day) resulting in a total cumulative dose of 210 mGy. Since 12 hours resting period between consecutive fractions would prevent induction of DNA damage response (because of DNA double strand break repair), but ROS generation can accumulate, one would assume that (7 x 30mGy) induces more lipid droplets as compared with 210 mGy or 3Gy applied in a single radiation exposure. This has indeed been found in my experiments. Moreover, I could also show that treating cells with the pro-LD dose of (6 x 30 mGy) on the last day with a single high dose of 3 Gy causes a rapid clearance of the LDs, most likely by efficiently triggering autophagy by the single high dose. In addition to a better understanding of the mechanisms that trigger autophagy in X-irradiated cells, the unexpected dose response has potential implications for radiation effects in patients as well. Doses of up to 30 mGy are typical in radiology imaging using computer tomography (CT). These low doses are normally considered harmless, and no cellular mechanism has been shown unequivocally to cause mutations, cell death or malignant transformation. The induction of lipid droplets as observed in my experiments with MSCs also might have little relevance for acute radiation damage to the tissue, nor for risk of induced secondary malignancies. But accumulating lipid toxicity after repeated X-ray irradiation, without the exposed cells triggering autophagy, might lead to more rapid cell ageing. The accumulation of damaged proteins and lipids after ROS stress has been clearly shown by others to be an important form of cellular stress associated with ageing.

4.6 Radiation can induce autophagy in Healthy BMSCs. Autophagy process is impaired in T2D-BMSCs

My results showed that after an (3 Gy) X-irradiation of 4 healthy donors derived primary BM-MSCs caused a response in terms of LDs and autophagy induction (measured by LC3B level) similar to what I already observed in the L87 cell line. As in the L87 cell line, the number of cells with LDs decreases after 3 Gy irradiation, whereas the LC3B signal increases by immunofluorescence.

The BM-MSCs derived from T2D donors, however, are significantly different in this assay. First of all, there is a higher LC3B signal already in the unirradiated control cells. The reason could be a permanently increased level of endogenous intracellular ROS level in T2D, related to oxidative stress and the chronic inflammation process in the patients. Studies have shown that the increase of AGEs(Yan et al., 2017), the activation of the oxidase signaling pathway of nicotinamide adenine dinucleotide phosphate (NADPH)(Kovac et al., 2015) and the increase of superoxide production in dysfunctional mitochondria(Roy Chowdhury et al., 2018) are all related to the overproduction of ROS induced by hyperglycemia. In addition, large amounts of ROS can cause irreversible damage to mitochondria, thus amplifying the initial oxidative stress response. The ROS produced by cells are increased, which promotes apoptosis and autophagy(L. Li et al., 2015). Because diabetic bone marrow stem cells are relatively precious and limited in number, the hypothesis cannot be verified and all experiments cannot be completed. We hoped that in the later stage, db/db diabetic mouse BMSCs can be used to verify the experiments again and for systematical study of related pathways.

Following X-irradiation, we found that autophagy occurred in healthy donors' BMSCs after radiation treatment, and LC3B signal of T2D donors showed autophagy resistance. Our conclusion is consistent with others, that T2D autophagy is impaired, which has not been found and reported in T2D BMSCs. This phenomenon further demonstrates the potential deficiency of T2D autologous stem cells in stem cell therapy. Therefore, by improving the autophagy ability of T2D autologous BMSCs,

efficacy of T2D autologous stem cells can be improved. There exist several possibilities to trigger autophagy: the straightest forward is a temporal nutrient restriction by starvation, which can be easily done in MSCs in cell culture, but also for the patient. Another possibility is the administration of establish pharmacologic inducers of autophagy, such as Rapamycin or Temsirolimus.

After 3 Gy X-irradiation, there was no indication of additional LC3B signal. Cells of 2 donors remain unchanged, and 2 other ones even show a drop of this autophagy related signal. This indicated inter-patient heterogeneity, but most likely an impairment of autophagy.

4.7 T2D-BMSCs showed more cells with lipid-droplets

Autophagy is a mechanism to maintain cell metabolic homeostasis, which is closely related to the degradation of various cellular contents. As a selective autophagy process, lipophagy can effectively identify and decompose lipid droplets. Lipophagy plays an important role in regulating lipid metabolism and preventing lipid deposition.

Autophagy is closely related to lipid metabolism, both of them depend on each other and restrict each other. Once the imbalance will cause occurrence of many diseases. The excess of fatty acids in cells will damage the scavenging function of autophagy. At the same time, the decrease of autophagy slows down fat degradation and increases intracellular lipid droplets accumulation, which increase autophagy load and damage autophagy function. Such a vicious circle leads to the occurrence of a variety of diseases, such as obesity, dyslipidemia, fatty liver and so on. In the study of hepatocytes, autophagy can remove lipid droplets accumulated in hepatocytes induced by energy stress and reduce lipid toxicity of hepatocytes, thus increasing their insulin sensitivity (S. W. Zhou et al., 2014). In general, on the one hand, autophagy can regulate lipid droplet degradation, and on the other hand, it can control lipid droplet formation. The precise regulatory mechanism is unclear.

Our results showed that autophagy level of T2D patients derived BMSCs was inhibited and a large number of lipid droplets were accumulated under radiation stress. This is consistent with the results of many studies that autophagy is impaired in T2D. This study strongly points to an impairment of cell macroautophagy in MSCs from T2D patients. Among other features of cellular stress, this can result in an accumulation of uncleared lipid droplets, as shown by the increase of oil-red O positive signals. I therefore propose that impaired autophagy at least in part underlies the reduced capacity of T2D derived MSCs in supporting tissue regeneration and wound healing.

4.8 T2D-BMSCs were accompanied by lower levels of senescence

Aging is a process of gradual biological impairment of normal body functions. This is accompanied by a decreased ability to respond to stress and an increased risk of morbidity and mortality. It has been found that the decrease of autophagy level in almost all cells and tissues is closely related to the aging phenotype of the organism and will lead to the further aggravation of senescence related diseases.

Senescence is an essential regulatory mechanism for cells to adapt to the internal and external environment. It can initiate autophagy, and autophagy ability also gradually decline in the process of senescence. Moderate enhancement of autophagy can delay senescence. Studies have shown that with increasing expression of autophagy protein ATG5, the anti-aging ability of mice was enhanced. The possible mechanism is that the enhanced autophagy increases the immune response and the clearance of denaturing proteins or pathogens, and reduces the inflammatory response(Pyo et al., 2013). Tissue specific knockout of ATG gene is presented as premature senility(Rubinsztein et al., 2011). These findings suggest that the loss of autophagy is associated with senescence.

However, our results are different from those of other researchers. We found that the radiation-treated T2D-BMSCs showed fewer senescent cells. We thought this might

be related to the increased mortality of T2D-BMSCs after radiation. Unfortunately, we had insufficient cells to analyze the cell survival curve and verify it.

4.9 Autophagy resistance of T2D-MSCs was unrelated to DNA damage response

The pathogenesis of T2D is complex, which is mainly related to family genetic tendency, racial heterogeneity, insulin receptor defect, insulin receptor substrate damage, protein tyrosine phosphatase-related gene up-regulation, excessive immune-inflammatory response, lipid toxicity and mitochondrial damage(Fan et al., 2016). Many studies have confirmed that DNA damage associated to aging and metabolic diseases such as diabetes(I. Shimizu et al., 2014). Double strand breaks (DSBs) is one of the most lethal injuries in DNA damage. Failure to repair DSBs not only endangers the self-renewal and differentiation ability of cells, but also leads to chromosome instability and disease(Khalil et al., 2011).

When DSBs are sensed in mammalian cells, the ataxia-telangiectasia mutant protein (ATM) is involved in DNA damage response. The activated ATM causes rapid phosphorylation of H2AX to γH2AX, which in turn marks out DNA damage signals and accumulates repair proteins.

Previous studies in our laboratory found that the reduction of age-related H2AX lesions in BMSCs after radiation was due to impaired DNA damage response. The decrease of DNA damage response in aging BMSCs is due to a regulatory change in gradual loss of ATM pathway activity(Hladik et al., 2019).

Our results show that at 1.5 hours after 3 Gy of radiation, the level of γH2AX foci from T2D-BMSCs and healthy-BMSCs were all increased, compared with the control group. However, γH2AX foci formations after 1.5 hours haven’t shown any difference between T2D and healthy donors. It means that autophagy resistance of T2D-BMSCs is unrelated to DNA damage response.

5 Conclusion

The results of my studies show that MSCs from T2D patients in comparison with cells from healthy donors are affected by an impaired capacity to undergo autophagy as a pro-survival mechanism. This was seen by the reduced potential to induce LC3-II proteins after high dose X-irradiation and a higher level of lipid droplets. This defect of autophagy might at least in part be the underlying reason of chronic wound healing problems in the diabetic patients.

I also showed that normal MSCs have a biphasic response in their autophagy mechanism after exposed to oxidative stress as a consequence of X-irradiation. Whereas doses of 30 mGy (and repeated fractions of those) did not induced autophagy, but caused accumulation of lipid droplets and carbonylated lipids, doses of 300mGy and higher clearly triggered autophagy and resulted in a successful elimination of lipid droplets. This might warrant a careful planning of CT-imaging, and in particular if multiple CT-scans are performed could suggest a prophylactic treatment with autophagy inducers (such as rapamycin, temsirolimus, or nutrient fasting).

The impaired potential of T2D derived MSCs for autophagy might have consequences for a future cell based therapy of wound healing complications. A supplementation of superficial wound protection with allogenic MSCs (from healthy donors) or autologous MSCs (from patient themselves, after in vitro curing by re-sensitizing to autophagy or by iPS cells regeneration) might be a future strategy to support a successful wound healing process and prevent progression to an ulceration.

6 List of tables and figures

6.1 Tables

6.2 Figures

7. References

Amann, B., Ludemann, C., Ratei, R., & Schmidt-Lucke, J. A. (2009). [Autologous bone-marrow stem-cell transplantation for induction of arteriogenesis for limb salvage in critical limb ischaemia]. *Zentralbl Chir, 134*(4), 298-304.

Babu, P. S., Danilovich, N., & Sairam, M. R. (2001). Hormone-induced receptor gene splicing: enhanced expression of the growth factor type I follicle-stimulating hormone receptor motif in the developing mouse ovary as a new paradigm in growth regulation. *Endocrinology, 142*(1), 381-389.

Bao, X., Wang, J., Zhou, G., Aszodi, A., Schonitzer, V., Scherthan, H., Atkinson, M. J., & Rosemann, M. (2020). Extended in vitro culture of primary human mesenchymal stem cells downregulates Brca1-related genes and impairs DNA double-strand break recognition. *FEBS Open Bio*.

Benito-Cuesta, I., Diez, H., Ordonez, L., & Wandosell, F. (2017). Assessment of Autophagy in Neurons and Brain Tissue. *Cells, 6*(3).

Bizzozero, O. A., DeJesus, G., Callahan, K., & Pastuszyn, A. (2005). Elevated protein carbonylation in the brain white matter and gray matter of patients with multiple sclerosis. *J Neurosci Res, 81*(5), 687-695.

Bizzozero, O. A., & Zheng, J. (2009). Identification of major S-nitrosylated proteins in murine experimental autoimmune encephalomyelitis. *J Neurosci Res, 87*(13), 2881-2889.

Brasaemle, D. L., Barber, T., Kimmel, A. R., & Londos, C. (1997). Post-translational regulation of perilipin expression. Stabilization by stored intracellular neutral lipids. *J Biol Chem, 272*(14), 9378-9387.

Brunk, U. T., & Terman, A. (2002). The mitochondrial-lysosomal axis theory of aging: accumulation of damaged mitochondria as a result of imperfect autophagocytosis. *Eur J Biochem, 269*(8), 1996-2002.

Cao, Y., Sun, Z., Liao, L., Meng, Y., Han, Q., & Zhao, R. C. (2005). Human adipose tissue-derived stem cells differentiate into endothelial cells in vitro and improve postnatal neovascularization in vivo. *Biochem Biophys Res Commun, 332*(2), 370-379.

Capasso, S., Alessio, N., Squillaro, T., Di Bernardo, G., Melone, M. A., Cipollaro, M., Peluso, G., & Galderisi, U. (2015). Changes in autophagy, proteasome activity and metabolism to determine a specific signature for acute and chronic senescent mesenchymal stromal cells. *Oncotarget, 6*(37), 39457-39468.

Carames, B., Olmer, M., Kiosses, W. B., & Lotz, M. K. (2015). The relationship of autophagy defects to cartilage damage during joint aging in a mouse model. *Arthritis Rheumatol, 67*(6), 1568-1576.

Carames, B., Taniguchi, N., Otsuki, S., Blanco, F. J., & Lotz, M. (2010). Autophagy is a protective mechanism in normal cartilage, and its aging-related loss is linked with cell death and osteoarthritis. *Arthritis Rheum, 62*(3), 791-801.

Carames, B., Taniguchi, N., Seino, D., Blanco, F. J., D'Lima, D., & Lotz, M. (2012). Mechanical injury suppresses autophagy regulators and pharmacologic activation of autophagy results in chondroprotection. *Arthritis Rheum, 64*(4), 1182-1192.

Charnogursky, G. A., Emanuele, N. V., & Emanuele, M. A. (2014). Neurologic complications of diabetes. *Curr Neurol Neurosci Rep, 14*(7), 457.

Chen, L., Tredget, E. E., Wu, P. Y., & Wu, Y. (2008). Paracrine factors of mesenchymal stem cells recruit macrophages and endothelial lineage cells and enhance wound healing. *PLoS One, 3*(4), e1886.

Chorlay, A., & Thiam, A. R. (2018). An Asymmetry in Monolayer Tension Regulates Lipid Droplet Budding Direction. *Biophys J, 114*(3), 631-640.

Corselli, M., Chen, C. W., Sun, B., Yap, S., Rubin, J. P., & Peault, B. (2012). The tunica adventitia of human arteries and veins as a source of mesenchymal stem cells. *Stem Cells Dev, 21*(8), 1299-1308.

Cuervo, A. M., & Wong, E. (2014). Chaperone-mediated autophagy: roles in disease and aging. *Cell Res, 24*(1), 92-104.

Dai, Y., Li, J., Li, J., Dai, G., Mu, H., Wu, Q., Hu, K., & Cao, Q. (2007). Skin epithelial cells in mice from umbilical cord blood mesenchymal stem cells. *Burns, 33*(4), 418-428.

Dalle-Donne, I., Giustarini, D., Colombo, R., Rossi, R., & Milzani, A. (2003). Protein carbonylation in human diseases. *Trends Mol Med, 9*(4), 169-176.

Dalle-Donne, I., Rossi, R., Colombo, R., Giustarini, D., & Milzani, A. (2006). Biomarkers of oxidative damage in human disease. *Clin Chem, 52*(4), 601-623.

Deretic, V., Saitoh, T., & Akira, S. (2013). Autophagy in infection, inflammation and immunity. *Nat Rev Immunol, 13*(10), 722-737.

Desta, T., Li, J., Chino, T., & Graves, D. T. (2010). Altered fibroblast proliferation and apoptosis in diabetic gingival wounds. *J Dent Res, 89*(6), 609-614.

Ding, Y., & Choi, M. E. (2015). Autophagy in diabetic nephropathy. *J Endocrinol, 224*(1), R15-30.

Fan, M., Li, W., Wang, L., Gu, S., Dong, S., Chen, M., Yin, H., Zheng, J., Wu, X., Jin, J., Jiang, X., Cai, J., Liu, P., & Zheng, C. (2016). Association of SLC30A8 gene polymorphism with type 2 diabetes, evidence from 46 studies: a meta-analysis. *Endocrine, 53*(2), 381-394.

Fernandez-Checa, J. C., Fernandez, A., Morales, A., Mari, M., Garcia-Ruiz, C., & Colell, A. (2010). Oxidative stress and altered mitochondrial function in neurodegenerative diseases: lessons from mouse models. *CNS Neurol Disord Drug Targets, 9*(4), 439-454.

Finn, P. F., & Dice, J. F. (2006). Proteolytic and lipolytic responses to starvation. *Nutrition, 22*(7-8), 830-844.

Gainza, G., Bonafonte, D. C., Moreno, B., Aguirre, J. J., Gutierrez, F. B., Villullas, S., Pedraz, J. L., Igartua, M., & Hernandez, R. M. (2015). The topical administration of rhEGF-loaded nanostructured lipid carriers (rhEGF-NLC) improves healing in a porcine full-thickness excisional wound model. *J Control Release, 197*, 41-47.

Gong, Y., Xiong, H., Du, Y., Wu, Y., Zhang, S., Li, X., & Liu, H. (2016). Autoantibodies against beta1-adrenoceptor induce blood glucose enhancement and insulin insufficient via T lymphocytes. *Immunol Res, 64*(2), 584-593.

Grootaert, M. O. J., Roth, L., Schrijvers, D. M., De Meyer, G. R. Y., & Martinet, W. (2018). Defective Autophagy in Atherosclerosis: To Die or to Senesce? *Oxid Med Cell Longev, 2018*, 7687083.

Gross, D. A., Zhan, C., & Silver, D. L. (2011). Direct binding of triglyceride to fat storage-inducing transmembrane proteins 1 and 2 is important for lipid droplet formation. *Proc Natl Acad Sci U S A, 108*(49), 19581-19586.

Han, Y. F., Sun, T. J., Han, Y. Q., Xu, G., Liu, J., & Tao, R. (2015). Clinical perspectives on mesenchymal stem cells promoting wound healing in diabetes mellitus patients by inducing autophagy. *Eur Rev Med Pharmacol Sci, 19*(14), 2666-2670.

Hashemi, H. F., & Goodman, J. M. (2015). The life cycle of lipid droplets. *Curr Opin Cell Biol, 33*, 119-124.

Hassan, M. I., Hammad, K. M., Fouda, M. A., & Kamel, M. R. (2014). The using of Lucilia cuprina maggots in the treatment of diabetic foot wounds. *J Egypt Soc Parasitol, 44*(1), 125-129.

Hayes, M., Choudhary, V., Ojha, N., Shin, J. J., Han, G. S., Carman, G. M., Loewen, C. J., Prinz, W. A., & Levine, T. (2017). Fat storage-inducing transmembrane (FIT or FITM) proteins are related to lipid phosphatase/phosphotransferase enzymes. *Microb Cell, 5*(2), 88-103.

He, C., & Klionsky, D. J. (2009). Regulation mechanisms and signaling pathways of autophagy. *Annu Rev Genet, 43*, 67-93.

Hladik, D., Hofig, I., Oestreicher, U., Beckers, J., Matjanovski, M., Bao, X., Scherthan, H., Atkinson, M. J., & Rosemann, M. (2019). Long-term culture of mesenchymal stem cells impairs ATM-dependent recognition of DNA breaks and increases genetic instability. *Stem Cell Res Ther, 10*(1), 218.

Hou, J., Han, Z. P., Jing, Y. Y., Yang, X., Zhang, S. S., Sun, K., Hao, C., Meng, Y., Yu, F. H., Liu, X. Q., Shi, Y. F., Wu, M. C., Zhang, L., & Wei, L. X. (2013). Autophagy prevents irradiation injury and maintains stemness through decreasing ROS generation in mesenchymal stem cells. *Cell Death Dis, 4*, e844.

Hu, Y. L., Jahangiri, A., Delay, M., & Aghi, M. K. (2012). Tumor cell autophagy as an adaptive response mediating resistance to treatments such as antiangiogenic therapy. *Cancer Res, 72*(17), 4294-4299.

Huang, E. J., Kuo, W. W., Chen, Y. J., Chen, T. H., Chang, M. H., Lu, M. C., Tzang, B. S., Hsu, H. H., Huang, C. Y., & Lee, S. D. (2006). Homocysteine and other biochemical parameters in Type 2 diabetes mellitus with different diabetic duration or diabetic retinopathy. *Clin Chim Acta, 366*(1-2), 293-298.

Imamura, M., Inoguchi, T., Ikuyama, S., Taniguchi, S., Kobayashi, K., Nakashima, N., & Nawata, H. (2002). ADRP stimulates lipid accumulation and lipid droplet formation in murine fibroblasts. *Am J Physiol Endocrinol Metab, 283*(4), E775-783.

Jeggo, P. A., & Lobrich, M. (2007). DNA double-strand breaks: their cellular and clinical impact? *Oncogene, 26*(56), 7717-7719.

Jiang, Y., Huang, S., Fu, X., Liu, H., Ran, X., Lu, S., Hu, D., Li, Q., Zhang, H., Li, Y., Wang, R., Xie, T., Cheng, B., Wang, L., Liu, Y., Ye, X., Han, C., & Chen, H. (2011). Epidemiology of chronic cutaneous wounds in China. *Wound Repair Regen, 19*(2), 181-188.

Jo, G. H., Bogler, O., Chwae, Y. J., Yoo, H., Lee, S. H., Park, J. B., Kim, Y. J., Kim, J. H., & Gwak, H. S. (2015). Radiation-induced autophagy contributes to cell death and induces apoptosis partly in malignant glioma cells. *Cancer Res Treat, 47*(2), 221-241.

Jude, E. B., Oyibo, S. O., Chalmers, N., & Boulton, A. J. (2001). Peripheral arterial disease in diabetic and nondiabetic patients: a comparison of severity and outcome. *Diabetes Care, 24*(8), 1433-1437.

Kajimura, S. (2015). Promoting brown and beige adipocyte biogenesis through the PRDM16 pathway. *Int J Obes Suppl, 5*(Suppl 1), S11-14.

Kakanj, P., Moussian, B., Gronke, S., Bustos, V., Eming, S. A., Partridge, L., & Leptin, M. (2016). Insulin and TOR signal in parallel through FOXO and S6K to promote epithelial wound healing. *Nat Commun, 7*, 12972.

Kang, M. A., So, E. Y., Simons, A. L., Spitz, D. R., & Ouchi, T. (2012). DNA damage induces reactive

oxygen species generation through the H2AX-Nox1/Rac1 pathway. *Cell Death Dis, 3*, e249.

Katsilambros N, D. E., Makrilakis K, Tentolouris N, Tsapogas P. (2010). Atlas of the diabetic foot. *2nd ed. Oxford: Wiley-Blackwell*.

Khalil, A., Morgan, R. N., Adams, B. R., Golding, S. E., Dever, S. M., Rosenberg, E., Povirk, L. F., & Valerie, K. (2011). ATM-dependent ERK signaling via AKT in response to DNA double-strand breaks. *Cell Cycle, 10*(3), 481-491.

Kim, H., Han, J. W., Lee, J. Y., Choi, Y. J., Sohn, Y. D., Song, M., & Yoon, Y. S. (2015). Diabetic Mesenchymal Stem Cells Are Ineffective for Improving Limb Ischemia Due to Their Impaired Angiogenic Capability. *Cell Transplant, 24*(8), 1571-1584.

Kim, K. A., Shin, D., Kim, J. H., Shin, Y. J., Rajanikant, G. K., Majid, A., Baek, S. H., & Bae, O. N. (2018). Role of Autophagy in Endothelial Damage and Blood-Brain Barrier Disruption in Ischemic Stroke. *Stroke, 49*(6), 1571-1579.

Kim, S. W., Sung, I. H., & Kim, Y. H. (2018). Reconstruction of severe atherosclerotic and obstructive diabetic feet using thoracodorsal artery perforator flaps with long vascular pedicles. *Microsurgery, 38*(3), 287-294.

Kim, W. S., Park, B. S., Sung, J. H., Yang, J. M., Park, S. B., Kwak, S. J., & Park, J. S. (2007). Wound healing effect of adipose-derived stem cells: a critical role of secretory factors on human dermal fibroblasts. *J Dermatol Sci, 48*(1), 15-24.

Kim, Y. C., & Guan, K. L. (2015). mTOR: a pharmacologic target for autophagy regulation. *J Clin Invest, 125*(1), 25-32.

Klionsky, D. J. (2007). Autophagy: from phenomenology to molecular understanding in less than a decade. *Nat Rev Mol Cell Biol, 8*(11), 931-937.

Kovac, S., Angelova, P. R., Holmstrom, K. M., Zhang, Y., Dinkova-Kostova, A. T., & Abramov, A. Y. (2015). Nrf2 regulates ROS production by mitochondria and NADPH oxidase. *Biochim Biophys Acta, 1850*(4), 794-801.

Kumar, S., Ashe, H. A., Parnell, L. N., Fernando, D. J., Tsigos, C., Young, R. J., Ward, J. D., & Boulton, A. J. (1994). The prevalence of foot ulceration and its correlates in type 2 diabetic patients: a population-based study. *Diabet Med, 11*(5), 480-484.

Kundu, M., & Thompson, C. B. (2008). Autophagy: basic principles and relevance to disease. *Annu Rev Pathol, 3*, 427-455.

Kurz, D. J., Decary, S., Hong, Y., & Erusalimsky, J. D. (2000). Senescence-associated (beta)-galactosidase reflects an increase in lysosomal mass during replicative ageing of human endothelial cells. *J Cell Sci, 113 (Pt 20)*, 3613-3622.

Larsen, L., Tchanque-Fossuo, C. N., Gorouhi, F., Boudreault, D., Nguyen, C., Fuentes, J. J., Crawford, R. W., Dahle, S. E., Whetzel, T., & Isseroff, R. R. (2018). Combination therapy of autologous adipose mesenchymal stem cell-enriched, high-density lipoaspirate and topical timolol for healing chronic wounds. *J Tissue Eng Regen Med, 12*(1), 186-190.

Lataillade, J. J., Doucet, C., Bey, E., Carsin, H., Huet, C., Clairand, I., Bottollier-Depois, J. F., Chapel, A., Ernou, I., Gourven, M., Boutin, L., Hayden, A., Carcamo, C., Buglova, E., Joussemet, M., de Revel, T., & Gourmelon, P. (2007). New approach to radiation burn treatment by dosimetry-guided surgery combined with autologous mesenchymal stem cell therapy. *Regen Med, 2*(5), 785-794.

Lee, T. G., Kim, S. Y., Kim, H. R., Kim, H., & Kim, C. H. (2020). Radiation Induces Autophagy via Histone H4 Lysine 20 Trimethylation in Non-small Cell Lung Cancer Cells. *Anticancer Res,*

40(5), 2537-2548.

Lee, Y. K., & Lee, J. A. (2016). Role of the mammalian ATG8/LC3 family in autophagy: differential and compensatory roles in the spatiotemporal regulation of autophagy. *BMB Rep, 49*(8), 424-430.

Leidal, A. M., Levine, B., & Debnath, J. (2018). Autophagy and the cell biology of age-related disease. *Nat Cell Biol, 20*(12), 1338-1348.

Li, J., Zhou, J., Zhang, D., Song, Y., She, J., & Bai, C. (2015). Bone marrow-derived mesenchymal stem cells enhance autophagy via PI3K/AKT signalling to reduce the severity of ischaemia/reperfusion-induced lung injury. *J Cell Mol Med, 19*(10), 2341-2351.

Li, L., Tan, J., Miao, Y., Lei, P., & Zhang, Q. (2015). ROS and Autophagy: Interactions and Molecular Regulatory Mechanisms. *Cell Mol Neurobiol, 35*(5), 615-621.

Li, P., & Guo, X. (2018). A review: therapeutic potential of adipose-derived stem cells in cutaneous wound healing and regeneration. *Stem Cell Res Ther, 9*(1), 302.

Li, Y., Qin, R., Yan, H., Wang, F., Huang, S., Zhang, Y., Zhong, M., Zhang, W., & Wang, Z. (2018). Inhibition of vascular smooth muscle cells premature senescence with rutin attenuates and stabilizes diabetic atherosclerosis. *J Nutr Biochem, 51*, 91-98.

Lindley, L. E., Stojadinovic, O., Pastar, I., & Tomic-Canic, M. (2016). Biology and Biomarkers for Wound Healing. *Plast Reconstr Surg, 138*(3 Suppl), 18S-28S.

Liu, W. J., Huang, W. F., Ye, L., Chen, R. H., Yang, C., Wu, H. L., Pan, Q. J., & Liu, H. F. (2018). The activity and role of autophagy in the pathogenesis of diabetic nephropathy. *Eur Rev Med Pharmacol Sci, 22*(10), 3182-3189.

Liu, X., Hao, W., Qin, Y., Decker, Y., Wang, X., Burkart, M., Schotz, K., Menger, M. D., Fassbender, K., & Liu, Y. (2015). Long-term treatment with Ginkgo biloba extract EGb 761 improves symptoms and pathology in a transgenic mouse model of Alzheimer's disease. *Brain Behav Immun, 46*, 121-131.

Lodge, A., Jones, M., & Thomas, S. (2006). Maggots 'n' chips: a novel approach to the treatment of diabetic ulcers. *Br J Community Nurs, 11*(12), suppl 23-26.

Lundin, C., Nordstrom, R., Wagner, K., Windpassinger, C., Andersson, H., von Heijne, G., & Nilsson, I. (2006). Membrane topology of the human seipin protein. *FEBS Lett, 580*(9), 2281-2284.

Madeo, F., Zimmermann, A., Maiuri, M. C., & Kroemer, G. (2015). Essential role for autophagy in life span extension. *J Clin Invest, 125*(1), 85-93.

Mizushima, N., & Klionsky, D. J. (2007). Protein turnover via autophagy: implications for metabolism. *Annu Rev Nutr, 27*, 19-40.

Mizushima, N., Levine, B., Cuervo, A. M., & Klionsky, D. J. (2008). Autophagy fights disease through cellular self-digestion. *Nature, 451*(7182), 1069-1075.

Mizushima, N., Yoshimori, T., & Ohsumi, Y. (2011). The role of Atg proteins in autophagosome formation. *Annu Rev Cell Dev Biol, 27*, 107-132.

Molaei, S., Roudkenar, M. H., Amiri, F., Harati, M. D., Bahadori, M., Jaleh, F., Jalili, M. A., & Mohammadi Roushandeh, A. (2015). Down-regulation of the autophagy gene, ATG7, protects bone marrow-derived mesenchymal stem cells from stressful conditions. *Blood Res, 50*(2), 80-86.

Mu, Y., Yan, R., Hu, X., He, J., Liu, H., & Li, Q. (2015). Levels of serum superoxide dismutase and high sensitive C-reactive protein in type 2 diabetic patients with lower extremity vascular disease are enhanced by interventional treatment. *Int J Clin Exp Med, 8*(1), 1540-1545.

Oliver, C. N., Ahn, B. W., Moerman, E. J., Goldstein, S., & Stadtman, E. R. (1987). Age-related changes in oxidized proteins. *J Biol Chem, 262*(12), 5488-5491.

Oliver, L., Hue, E., Priault, M., & Vallette, F. M. (2012). Basal autophagy decreased during the differentiation of human adult mesenchymal stem cells. *Stem Cells Dev, 21*(15), 2779-2788.

Oliver, L., Hue, E., Rossignol, J., Bougras, G., Hulin, P., Naveilhan, P., Heymann, D., Lescaudron, L., & Vallette, F. M. (2011). Distinct roles of Bcl-2 and Bcl-Xl in the apoptosis of human bone marrow mesenchymal stem cells during differentiation. *PLoS One, 6*(5), e19820.

Olzmann, J. A., & Carvalho, P. (2019). Dynamics and functions of lipid droplets. *Nat Rev Mol Cell Biol, 20*(3), 137-155.

Orozco-Beltran, D., Mata-Cases, M., Artola, S., Conthe, P., Mediavilla, J., & Miranda, C. (2016). [Adherence of Type 2 Diabetes Mellitus approach: Current situation and possible solutions]. *Aten Primaria, 48*(6), 406-420.

Paglin, S., Hollister, T., Delohery, T., Hackett, N., McMahill, M., Sphicas, E., Domingo, D., & Yahalom, J. (2001). A novel response of cancer cells to radiation involves autophagy and formation of acidic vesicles. *Cancer Res, 61*(2), 439-444.

Pan H-Z, Z. L., Guo M-Y, et al. (2010). The oxidative stress status in diabetes mellitus and diabetic nephropathy. *Acta Diabetol, 47*(Suppl 1), 71–76.

Paull, T. T., Rogakou, E. P., Yamazaki, V., Kirchgessner, C. U., Gellert, M., & Bonner, W. M. (2000). A critical role for histone H2AX in recruitment of repair factors to nuclear foci after DNA damage. *Curr Biol, 10*(15), 886-895.

Pforringer, D., Aitzetmuller, M. M., Brett, E. A., Houschyar, K. S., Schafer, R., van Griensven, M., & Duscher, D. (2018). Single-Cell Gene Expression Analysis and Evaluation of the Therapeutic Function of Murine Adipose-Derived Stromal Cells (ASCs) from the Subcutaneous and Visceral Compartment. *Stem Cells Int, 2018*, 2183736.

Pol, A., Gross, S. P., & Parton, R. G. (2014). Review: biogenesis of the multifunctional lipid droplet: lipids, proteins, and sites. *J Cell Biol, 204*(5), 635-646.

Pyo, J. O., Yoo, S. M., Ahn, H. H., Nah, J., Hong, S. H., Kam, T. I., Jung, S., & Jung, Y. K. (2013). Overexpression of Atg5 in mice activates autophagy and extends lifespan. *Nat Commun, 4*, 2300.

Rao, M., Gao, C., Xu, L., Jiang, L., Zhu, J., Chen, G., Law, B. Y. K., & Xu, Y. (2019). Effect of Inulin-Type Carbohydrates on Insulin Resistance in Patients with Type 2 Diabetes and Obesity: A Systematic Review and Meta-Analysis. *J Diabetes Res, 2019*, 5101423.

Rehman, J., Traktuev, D., Li, J., Merfeld-Clauss, S., Temm-Grove, C. J., Bovenkerk, J. E., Pell, C. L., Johnstone, B. H., Considine, R. V., & March, K. L. (2004). Secretion of angiogenic and antiapoptotic factors by human adipose stromal cells. *Circulation, 109*(10), 1292-1298.

Ren, S., Chen, J., Duscher, D., Liu, Y., Guo, G., Kang, Y., Xiong, H., Zhan, P., Wang, Y., Wang, C., Machens, H. G., & Chen, Z. (2019). Microvesicles from human adipose stem cells promote wound healing by optimizing cellular functions via AKT and ERK signaling pathways. *Stem Cell Res Ther, 10*(1), 47.

Revuelta, M., & Matheu, A. (2017). Autophagy in stem cell aging. *Aging Cell, 16*(5), 912-915.

Robenek, H., Robenek, M. J., & Troyer, D. (2005). PAT family proteins pervade lipid droplet cores. *J Lipid Res, 46*(6), 1331-1338.

Rodriguez-Vargas, J. M., Ruiz-Magana, M. J., Ruiz-Ruiz, C., Majuelos-Melguizo, J., Peralta-Leal, A., Rodriguez, M. I., Munoz-Gamez, J. A., de Almodovar, M. R., Siles, E., Rivas, A. L., Jaattela,

M., & Oliver, F. J. (2012). ROS-induced DNA damage and PARP-1 are required for optimal induction of starvation-induced autophagy. *Cell Res, 22*(7), 1181-1198.

Roy Chowdhury, S., Djordjevic, J., Thomson, E., Smith, D. R., Albensi, B. C., & Fernyhough, P. (2018). Depressed mitochondrial function and electron transport Complex II-mediated H2O2 production in the cortex of type 1 diabetic rodents. *Mol Cell Neurosci, 90*, 49-59.

Rubinsztein, D. C., Marino, G., & Kroemer, G. (2011). Autophagy and aging. *Cell, 146*(5), 682-695.

Sahu, R., Kaushik, S., Clement, C. C., Cannizzo, E. S., Scharf, B., Follenzi, A., Potolicchio, I., Nieves, E., Cuervo, A. M., & Santambrogio, L. (2011). Microautophagy of cytosolic proteins by late endosomes. *Dev Cell, 20*(1), 131-139.

Santambrogio, L., & Cuervo, A. M. (2011). Chasing the elusive mammalian microautophagy. *Autophagy, 7*(6), 652-654.

Sanyal, A. J., Campbell-Sargent, C., Mirshahi, F., Rizzo, W. B., Contos, M. J., Sterling, R. K., Luketic, V. A., Shiffman, M. L., & Clore, J. N. (2001). Nonalcoholic steatohepatitis: association of insulin resistance and mitochondrial abnormalities. *Gastroenterology, 120*(5), 1183-1192.

Shaw, J. E., Sicree, R. A., & Zimmet, P. Z. (2010). Global estimates of the prevalence of diabetes for 2010 and 2030. *Diabetes Res Clin Pract, 87*(1), 4-14.

Shimizu, I., Yoshida, Y., Suda, M., & Minamino, T. (2014). DNA damage response and metabolic disease. *Cell Metab, 20*(6), 967-977.

Shimizu, S., Yoshida, T., Tsujioka, M., & Arakawa, S. (2014). Autophagic cell death and cancer. *Int J Mol Sci, 15*(2), 3145-3153.

Shin, L., & Peterson, D. A. (2012). Impaired therapeutic capacity of autologous stem cells in a model of type 2 diabetes. *Stem Cells Transl Med, 1*(2), 125-135.

Sim, M. F., Talukder, M. U., Dennis, R. J., Edwardson, J. M., & Rochford, J. J. (2014). Analyzing the functions and structure of the human lipodystrophy protein seipin. *Methods Enzymol, 537*, 161-175.

Singh, R., Kaushik, S., Wang, Y., Xiang, Y., Novak, I., Komatsu, M., Tanaka, K., Cuervo, A. M., & Czaja, M. J. (2009). Autophagy regulates lipid metabolism. *Nature, 458*(7242), 1131-1135.

Stankov, M. V., Panayotova-Dimitrova, D., Leverkus, M., Vondran, F. W., Bauerfeind, R., Binz, A., & Behrens, G. M. (2012). Autophagy inhibition due to thymidine analogues as novel mechanism leading to hepatocyte dysfunction and lipid accumulation. *AIDS, 26*(16), 1995-2006.

Sung, I. H., Jang, D. W., Kim, S. W., Kim, Y. H., & Kim, S. W. (2018). Reconstruction of diabetic lower leg and foot soft tissue defects using thoracodorsal artery perforator chimeric flaps. *Microsurgery, 38*(6), 674-681.

Suomi, F., & McWilliams, T. G. (2019). Autophagy in the mammalian nervous system: a primer for neuroscientists. *Health Psychol Behav Med, 3*(3), NS20180134.

Switon, K., Kotulska, K., Janusz-Kaminska, A., Zmorzynska, J., & Jaworski, J. (2017). Molecular neurobiology of mTOR. *Neuroscience, 341*, 112-153.

Tanida, I., Minematsu-Ikeguchi, N., Ueno, T., & Kominami, E. (2005). Lysosomal turnover, but not a cellular level, of endogenous LC3 is a marker for autophagy. *Autophagy, 1*(2), 84-91.

Tesfaye, S., Stevens, L. K., Stephenson, J. M., Fuller, J. H., Plater, M., Ionescu-Tirgoviste, C., Nuber, A., Pozza, G., & Ward, J. D. (1996). Prevalence of diabetic peripheral neuropathy and its relation to glycaemic control and potential risk factors: the EURODIAB IDDM Complications Study. *Diabetologia, 39*(11), 1377-1384.

Thalmeier, K., Meissner, P., Moosmann, S., Sagebiel, S., Wiest, I., & Huss, R. (2001). Mesenchymal

differentiation and organ distribution of established human stromal cell lines in NOD/SCID mice. *Acta Haematol, 105*(3), 159-165.

Tra, T., Gong, L., Kao, L. P., Li, X. L., Grandela, C., Devenish, R. J., Wolvetang, E., & Prescott, M. (2011). Autophagy in human embryonic stem cells. *PLoS One, 6*(11), e27485.

Usui, M. L., Mansbridge, J. N., Carter, W. G., Fujita, M., & Olerud, J. E. (2008). Keratinocyte migration, proliferation, and differentiation in chronic ulcers from patients with diabetes and normal wounds. *J Histochem Cytochem, 56*(7), 687-696.

van de Vyver, M. (2017). Intrinsic Mesenchymal Stem Cell Dysfunction in Diabetes Mellitus: Implications for Autologous Cell Therapy. *Stem Cells Dev, 26*(14), 1042-1053.

Vincent, A. M., Callaghan, B. C., Smith, A. L., & Feldman, E. L. (2011). Diabetic neuropathy: cellular mechanisms as therapeutic targets. *Nat Rev Neurol, 7*(10), 573-583.

Wang, C., Telpoukhovskaia, M. A., Bahr, B. A., Chen, X., & Gan, L. (2018). Endo-lysosomal dysfunction: a converging mechanism in neurodegenerative diseases. *Curr Opin Neurobiol, 48*, 52-58.

Wang, D., Kreutzer, D. A., & Essigmann, J. M. (1998). Mutagenicity and repair of oxidative DNA damage: insights from studies using defined lesions. *Mutat Res, 400*(1-2), 99-115.

Wang, L., Ye, X., & Zhao, T. (2019). The physiological roles of autophagy in the mammalian life cycle. *Biol Rev Camb Philos Soc, 94*(2), 503-516.

Wang, X., Zhou, X., Ma, J., Tian, H., Jiao, Y., Zhang, R., Huang, Z., Xiao, J., Zhao, B., Qian, H., & Li, X. (2010). Effects of keratinocyte growth factor-2 on corneal epithelial wound healing in a rabbit model of carbon dioxide laser injury. *Biol Pharm Bull, 33*(6), 971-976.

Wilfling, F., Haas, J. T., Walther, T. C., & Farese, R. V., Jr. (2014). Lipid droplet biogenesis. *Curr Opin Cell Biol, 29*, 39-45.

Xu, F., Hua, C., Tautenhahn, H. M., Dirsch, O., & Dahmen, U. (2020). The Role of Autophagy for the Regeneration of the Aging Liver. *Int J Mol Sci, 21*(10).

Yan, X., Wu, H., Wu, Z., Hua, F., Liang, D., Sun, H., Yang, Y., Huang, D., & Bian, J. S. (2017). The New Synthetic H2S-Releasing SDSS Protects MC3T3-E1 Osteoblasts against H2O2-Induced Apoptosis by Suppressing Oxidative Stress, Inhibiting MAPKs, and Activating the PI3K/Akt Pathway. *Front Pharmacol, 8*, 07.

Yang, H., Lian, D., Zhang, X., Li, H., & Xin, G. (2019). Key Genes and Signaling Pathways Contribute to the Pathogensis of Diabetic Nephropathy. *Iran J Kidney Dis, 13*(2), 87-97.

Yu, J., & Li, P. (2017). The size matters: regulation of lipid storage by lipid droplet dynamics. *Sci China Life Sci, 60*(1), 46-56.

Zhang, D., Tang, B., Xie, X., Xiao, Y. F., Yang, S. M., & Zhang, J. W. (2015). The interplay between DNA repair and autophagy in cancer therapy. *Cancer Biol Ther, 16*(7), 1005-1013.

Zheng, J., & Bizzozero, O. A. (2010). Traditional reactive carbonyl scavengers do not prevent the carbonylation of brain proteins induced by acute glutathione depletion. *Free Radic Res, 44*(3), 258-266.

Zhou, L., Ma, B., & Han, X. (2016). The role of autophagy in angiotensin II-induced pathological cardiac hypertrophy. *J Mol Endocrinol, 57*(4), R143-R152.

Zhou, S. W., Zhang, M., & Zhu, M. (2014). Liraglutide reduces lipid accumulation in steatotic L02 cells by enhancing autophagy. *Mol Med Rep, 10*(5), 2351-2357.

Zhou, X., Takatoh, J., & Wang, F. (2011). The mammalian class 3 PI3K (PIK3C3) is required for early embryogenesis and cell proliferation. *PLoS One, 6*(1), e16358.

Zimmermann, R., Strauss, J. G., Haemmerle, G., Schoiswohl, G., Birner-Gruenberger, R., Riederer, M., Lass, A., Neuberger, G., Eisenhaber, F., Hermetter, A., & Zechner, R. (2004). Fat mobilization in adipose tissue is promoted by adipose triglyceride lipase. *Science, 306*(5700), 1383-1386.

Zou, Z., Yuan, Z., Zhang, Q., Long, Z., Chen, J., Tang, Z., Zhu, Y., Chen, S., Xu, J., Yan, M., Wang, J., & Liu, Q. (2012). Aurora kinase A inhibition-induced autophagy triggers drug resistance in breast cancer cells. *Autophagy, 8*(12), 1798-1810.

Acknowledgments

The 3-year Dr. med phase in Germany is coming to an end. I really thank my 3 tutors ***(Prof. Dr. Hans-Günther Machens, Dr. Michael Rosemann, Prof. Dr. Michael J. Atkinson)*** and two large working families, department of Plastic surgery and hand surgery of Klinikum rechts der Isar and Institute of Radiation Biology, Helmholtz Center Munich. This makes me feel the meticulous love and care. I never feel lost or lonely because of being abroad. During this period, I learnt how to summarize the research results, research methods, etc., and how to adjust the pace of life and training to adapt to the scientific research work at the Dr. med phase.

First of all, I would like to thank my tutor ***Prof. Dr. Hans-Günther Machens***. Prof. Dr. Hans-Günther Machens is a very kind person. He always tries his best to give every student a good platform, resources, and an environment, protect their rights and interests, and think about the future development for them. He lets me find goals and role model for the future road.

Secondly, I would like to thank ***Dr. Michael Rosemann*** for his patient guidance. Whenever I encounter difficulties that I have never encountered, I can get key inspiration from him. Whenever I am confused about the way ahead, Dr. Michael Rosemann can give me instructions. He is more like a friend, take care of me and bringing joy at any times. Without him, I cannot work smoothly in this relatively loose experimental environment.

Then, I would like to thank ***Prof. Dr. Michael J. Atkinson***. He always smiles at everyone. During the monthly group meetings, everyone sat together and kept in a deeper discussion of each other's topic. The weekly journal club has taught me a lot of knowledge out of books and hospital experiments. Taking turns presenting, he gave me the opportunity to show myself, and found deficiencies improving myself.

I would like to thank ***Dr. Dominik Duscher.*** At the time of enrollment, I successfully solved the problem of changing the university, and he helped me set the research

direction with Dr. Michael Rosemann. Although I did not conduct experiments in the hospital laboratory, he emailed me regularly to follow my progress. I would like to thank ***Ms. Mateja Vodiskar***. She helped me a lot in handling all the documents. No matter when I send emails, I can get her prompt reply and she helped me solve all problems quickly.

I would like to thank technician, ***Ms. Stefanie Winkler***, who helped me draw illustrations in this dissertation.

I would like to thank China Scholarship Council for covering my three-year scholarship.

Finally, I want to thank **my parents and my husband** for their meticulous care and attention. After getting married, I made a request to study abroad. My husband did not hesitate to support my decision, and encouraged me whenever I encountered difficulties at any time.

During these three years in Germany, I spent a happy and memorable time.